SRI International

(12)

April 21, 1986

Technical Report No. 1

MODEL FOR THE STEADY-STATE ROTATIONAL STIMULATED RAMAN GAIN COEFFICIENTS IN THE ATMOSPHERE

By: G. C. Herring, William K. Bischel, M. J. Dyer, and D. L. Huestis

Prepared for:

OFFICE OF NAVAL RESEARCH
1030 E. Green Street
Pasadena, CA 91106

Attn: Dr. R. E. Behringer

Funded Under DARPA Order No. 3125

SRI Project No. 7123
Contract No. N00014-84-C-0256
MP 85-217

SRI International
333 Ravenswood Ave • Menlo Park CA 94025
415 326-6200 • TWX 910-373-2046 • Telex 334-486

Unclassified
SECURITY CLASSIFICATION OF THIS PAGE

AD-A167 469

REPORT DOCUMENTATION PAGE

1a. REPORT SECURITY CLASSIFICATION: Unclassified	1b. RESTRICTIVE MARKINGS
2a. SECURITY CLASSIFICATION AUTHORITY	3. DISTRIBUTION/AVAILABILITY OF REPORT: Distribution unlimited; approved for public release.
2b. DECLASSIFICATION/DOWNGRADING SCHEDULE	
4. PERFORMING ORGANIZATION REPORT NUMBER(S): MP 85-217	5. MONITORING ORGANIZATION REPORT NUMBER(S)
6a. NAME OF PERFORMING ORGANIZATION: SRI International; 6b. OFFICE SYMBOL (If applicable)	7a. NAME OF MONITORING ORGANIZATION: Office of Naval Research
6c. ADDRESS (City, State and ZIP Code): 333 Ravenswood Ave. Menlo Park, CA 94025	7b. ADDRESS (City, State and ZIP Code): 1030 E. Green Street Pasadena, CA 91106
8a. NAME OF FUNDING/SPONSORING ORGANIZATION: Defense Advanced Research Projects Agency; 8b. OFFICE SYMBOL (If applicable)	9. PROCUREMENT INSTRUMENT IDENTIFICATION NUMBER: Contract No. N00014-84-C-0256
8c. ADDRESS (City, State and ZIP Code): 1400 Wilson Boulevard Arlington, VA 22209	10. SOURCE OF FUNDING NOS. — PROGRAM ELEMENT NO. / PROJECT NO. / TASK NO. / WORK UNIT NO.

11. TITLE (Include Security Classification): Model for the Steady-State Rotational Stimulated Raman Gain Coefficients in the Atmosphere"

12. PERSONAL AUTHOR(S): W. K. Bischel, G. C. Herring, M. J. Dyer, D. L. Huestis

13a. TYPE OF REPORT	13b. TIME COVERED	14. DATE OF REPORT (Yr., Mo., Day)	15. PAGE COUNT
Technical	FROM _____ TO _____	1986 March 12	

16. SUPPLEMENTARY NOTATION

17 COSATI CODES			18 SUBJECT TERMS (Continue on reverse if necessary and identify by block number)
FIELD	GROUP	SUB. GR.	

19. ABSTRACT (Continue on reverse if necessary and identify by block number)

A model for stimulated Raman scattering in the atmosphere is described for the pure rotational transitions in N_2^7. An empirical formula for the wavelength dependence of the N_2 polarizability anisotropy is derived from published measurements. The temperature and density dependence of the Raman linewidths were also measured in the laboratory. These results were then used to calculate the steady-state, plane wave Raman gain coefficient over the lower 100 km of the atmosphere. At sea level, the strongest lines have gain coefficients of 0.7 km^{-1} cm^2 MW^{-1} for a Stokes laser wavelength of 350 nm.

20 DISTRIBUTION/AVAILABILITY OF ABSTRACT	21 ABSTRACT SECURITY CLASSIFICATION
UNCLASSIFIED/UNLIMITED ☒ SAME AS RPT. ☐ DTIC USERS ☐	Unclassified

22a. NAME OF RESPONSIBLE INDIVIDUAL	22b TELEPHONE NUMBER (Include Area Code)	22c OFFICE SYMBOL
Dr. R. E. Behringer	(818) 795-5971	

DD FORM 1473, 83 APR — EDITION OF 1 JAN 73 IS OBSOLETE

Unclassified
SECURITY CLASSIFICATION OF THIS PAGE

CONTENTS

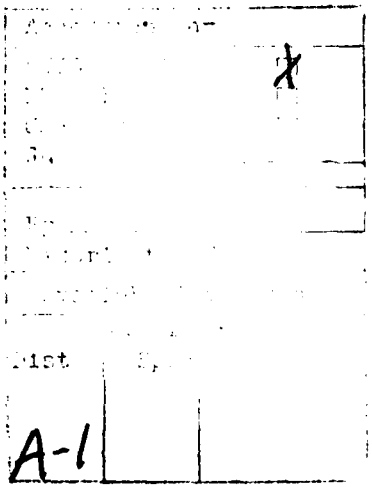

ILLUSTRATIONS

I INTRODUCTION

Stimulated Raman scattering will limit the maximum laser intensity that can be transmitted through the atmosphere if the divergence of the beam is required to remain constant. To establish this maximum intensity, it is necessary to obtain an accurate description of the steady-state Raman gain coefficient in the atmosphere. This report describes a model of the gain coefficient for the Stokes rotational transitions in N_2 under atmospheric conditions. This model is based on the results of laboratory measurements for the polarizability anisotropy, the density self-broadening coefficients, and the O_2 foreign-gas density broadening coefficients. These measurements are described in Appendices A and B and are used with a published atmospheric model[1] to calculate the Raman gain coefficient as a function of altitude from 0 to 100 km.

It should be emphasized here that the modeling of the propagation of a high intensity laser pulse through a Raman medium, such as the atmosphere, requires a propagation code that includes transient effects, off-axis propagation for the generated beams, the inclusion of all possible Stokes and anti-Stokes orders that can be generated, and the provision for a variable pump laser bandwidth. Codes including some of these effects are currently being developed in several laboratories. The model of the steady-state gain coefficient presented here will be an important input to these codes.

II MODEL DESCRIPTION

A. Atmospheric Model

In the atmospheric model, the Raman gain calculation uses the altitude-dependent temperature, N_2 density, and O_2 density as input data. The atmospheric model used here, given by Banks and Kockarts,[1] is for Wallops Island, Virginia (38^{o}N). Temperatures and densities for N_2 and O_2 were taken from Table 3.1 of Reference 1. Densities were extrapolated for the first 15 km (omitted from Table 3.1 of Reference 1) by assuming an exponential decay with increasing altitude, an e^{-1} altitude of 8 km, and relative densities of 78% and 21% for N_2 and O_2, respectively. The average temperature profiles for summer and winter are shown in Figure 1. Maximum variations are indicated by horizontal bars for summer and by shading for winter. Temperatures for the first 15 km (also omitted from Reference 1) were determined from the average of the summer and winter values in Figure 1.

B. Raman Gain Model

The steady-state, plane wave Raman gain coefficient is given by[2]

$$g = \frac{\lambda_s^2 \, \Delta N}{h\nu_s} \frac{\partial\sigma}{\partial\Omega} f(\delta\nu) \qquad (1)$$

where $f(\delta\nu)$ is the area-normalized Raman lineshape and $\delta\nu = \nu_p - \nu_s - \nu_R$, where $\nu_{p,s}$ is the pump/Stokes laser frequencies, ν_R is the Raman transition frequency, and ΔN is the population difference as specified in Appendix A. At the peak ($\delta\nu = 0$) of a Lorentzian-shaped transition, equation (1) from above reduces to equation (1) of Appendix A. This study uses equation (1) to calculate the Raman gain coefficient; hence the spontaneous scattering cross section, $\partial\sigma/\partial\Omega$, and the lineshape, $f(\delta\nu)$, must first be determined.

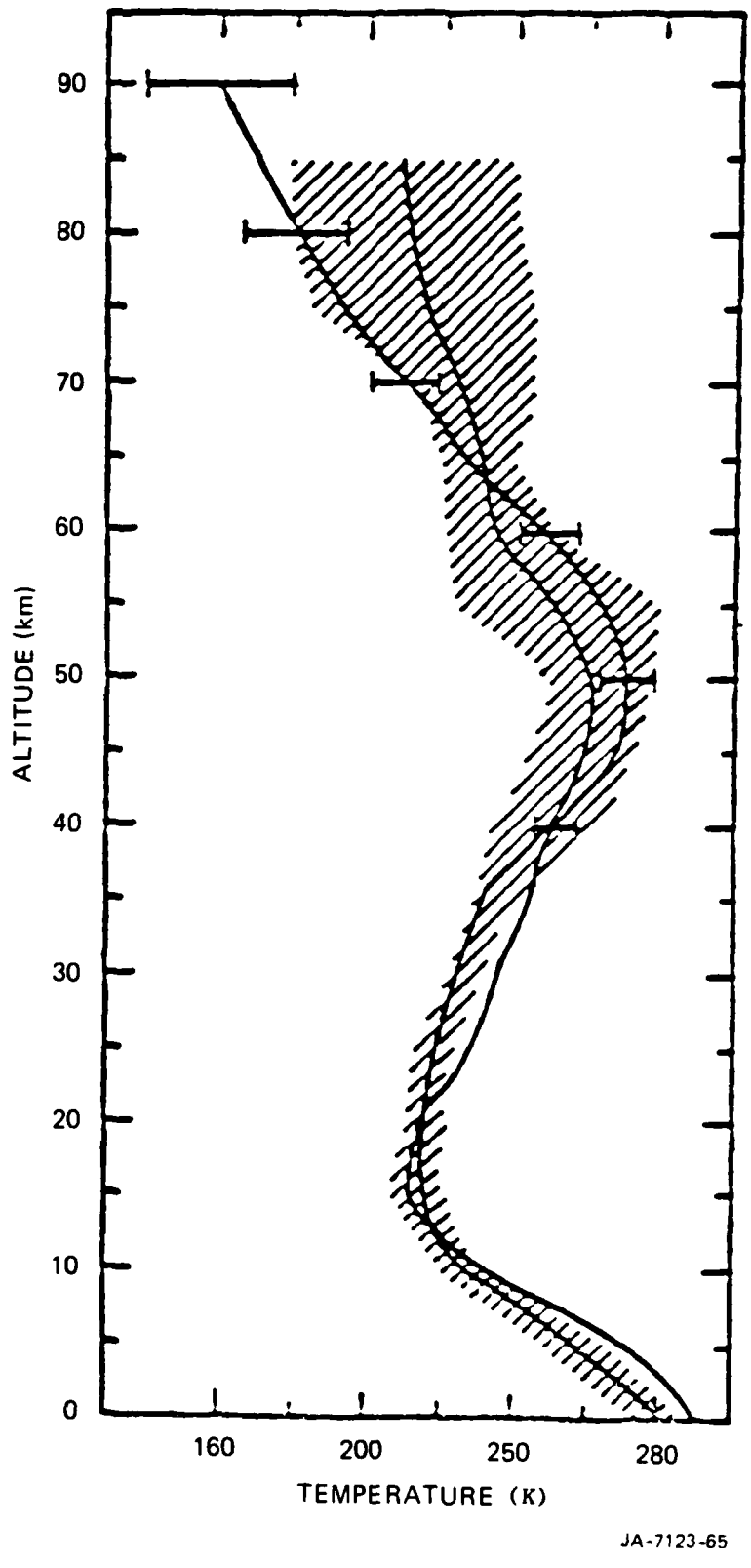

FIGURE 1 TEMPERATURE PROFILES USED IN THE RAMAN GAIN CALCULATIONS. Maximum variations are indicated by horizontal bars for summer and by shading for winter (after Ref. 1).

The cross section, $\partial\sigma/\partial\Omega$ is given by equation (2) of Appendix A. This expression contains the polarizability anisotropy, γ, which is given by equation (3) of Appendix A and reproduced here:

$$\gamma = \alpha_{s\parallel}\left(\frac{\nu_{i\parallel}^2}{\nu_{i\parallel}^2 - \nu^2}\right) - \alpha_{s\perp}\left(\frac{\nu_{i\perp}^2}{\nu_{i\perp}^2 - \nu^2}\right) \qquad (2)$$

The parameters $\alpha_{s\parallel}$, $\alpha_{s\perp}$, $\nu_{i\parallel}$, and $\nu_{i\perp}$ and the procedure used to determine them are also given in Appendix A. The wavelength dependence of equation (2) is shown as a solid line in Figure 2 along with several experimental values.[2-6] Note that the solid line is not a direct fit to the data points, but is derived according to the procedure described in Appendix A. For N_2, the J dependence of the polarizability anisotropy is < 1% for $0 < J < 20$ and is neglected. Equation (2) gives a value of 7.39×10^{-25} cm^3 for $\lambda_s = 350$ nm. All gain results presented in this report (except those in Appendix A) are for $\lambda_s = 350$ nm.

The accuracy of equation (2) can be checked by using the parameters $\nu_{i\parallel}$, $\nu_{i\perp}$, $\alpha_{s\parallel}$, and $\alpha_{s\perp}$ to calculate the index of refraction, n. The results can then be compared with experimental data[7] for n-1:

$$\frac{2}{3}(n-1) \simeq \frac{n^2-1}{n^2+2} = \frac{4\pi N}{9}\left[\frac{\nu_{i\parallel}^2\,\alpha_{s\parallel}}{\nu_{i\parallel}^2 - \nu^2} + \frac{2\nu_{i\perp}^2\,\alpha_{s\perp}}{\nu_{i\perp}^2 - \nu^2}\right] \qquad (3)$$

This comparison is made in Figure 3, where the dashed line shows our current model and the triangles show the experimental data from the literature. The agreement is excellent, with the largest discrepancy for (n - 1) being about 0.5%. Figure 3 illustrates the high accuracy reported in Appendix A for the polarizability anisotropy of equation (2).

The population difference, ΔN, was calculated using a N_2 rotational constant of 1.99 cm^{-1}. More accurate coefficients can be found in Reference 8.

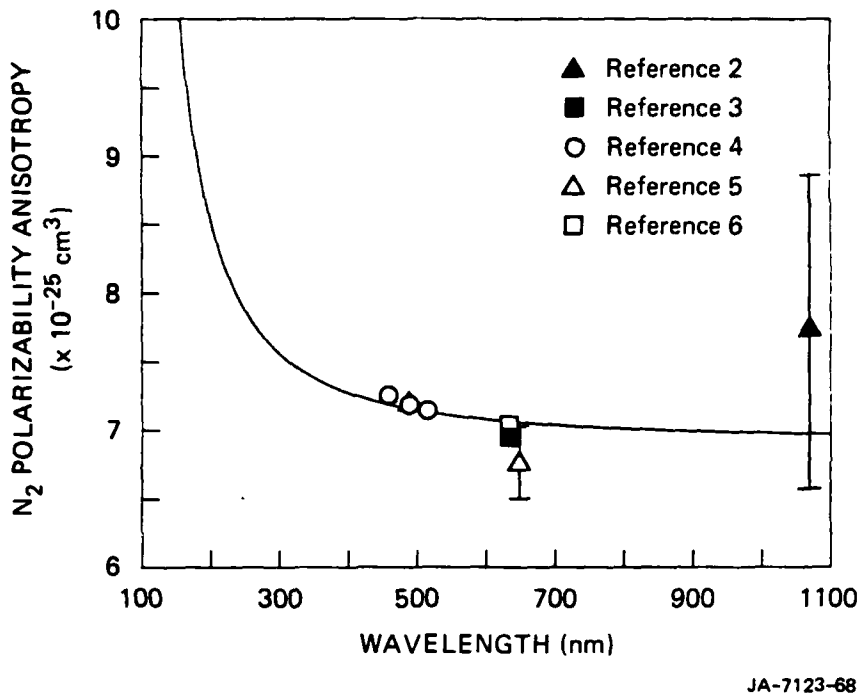

FIGURE 2 WAVELENGTH DEPENDENCE OF THE POLARIZABILITY ANISOTROPY DETERMINED FROM LEAST SQUARES FITS TO THE AVAILABLE EXPERIMENTAL DATA (INDIVIDUAL POINTS). See Appendix A for the procedure used to generate the fit (solid line).

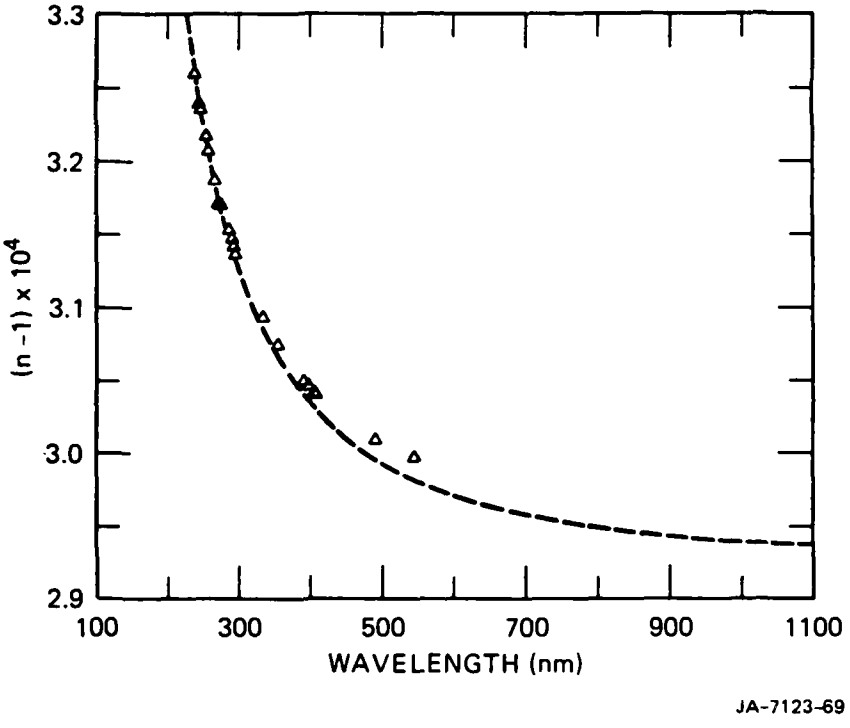

FIGURE 3 COMPARISON OF THE EXPERIMENTAL DATA (Δ) FROM REF. 7 AND THE RESULTS OF OUR MODEL (DASHED LINE) FOR THE INDEX OF REFRACTION, n.

Pure Voigt lineshapes were used for all results presented here. The width of the Lorentzian contribution to the Voigt was obtained by adding the linewidths due to self-broadening and foreign-gas broadening due to O_2. The present linewidth measurements as a function of temperature and density are summarized in Appendix B. Self-broadening coefficients not given in Table I of Appendix B were determined by assuming a linear J dependence. Foreign-gas broadening coefficients for temperatures and J's not given in Table V of Appendix B were determined by assuming the foreign-gas values are 85% of the corresponding self-broadening values in Table I of Appendix B. In this study, all broadening coefficients from Appendix B were assumed to vary linearly with temperature.

Only Gaussian laser lineshapes were considered for this model. Thus, the linewidth of the Gaussian component for the Voigt profile was determined from the square root of the sum of the squares of the laser and Doppler linewidths. After the Lorentzian and Gaussian linewidths were determined, an area-normalized Voigt calculation was used to determine $f(\delta\nu)$ in equation (1).

III RESULTS

A. Altitude Dependence

Figure 4 shows the peak Raman gain coefficient as a function of altitude for S(8). For comparison, the dotted line shows the gain if the approximation $\Delta\nu_T^2 = \Delta\nu_G^2 + \Delta\nu_L^2$ is used with equation (1) of Appendix A. The quantities $\delta\nu_T$, $\Delta\nu_G$, and $\Delta\nu_L$ are the total, Gaussian, and Lorentzian FWHM linewidths, respectively. The two quantities ΔN and $\Delta\nu_T$ that produce this altitude profile are also shown as functions of altitude in Figures 5 and 6. The Raman gain of Figure 4 is approximately constant below 40 km and drops to zero above 40 km. This occurs because the peak Raman gain depends on the ratio $\Delta N/\Delta\nu_T$. Below 40 km, Figures 5 and 6 show that ΔN and $\Delta\nu_T$ decrease with altitude at about the same rate, yielding a constant value of gain. Above 40 km, Figure 6 shows that $\Delta\nu_T$ becomes constant, whereas Figure 5 shows ΔN continues to decrease; thus, the Raman gain also decreases. The Raman linewidth is constant at high altitudes because the collisional broadening becomes negligible compared with the roughly constant Doppler broadening.

The peak Raman gain coefficients for the strongest Stokes transitions are shown as a function of altitude in Figure 7. The number indicated next to each curve is the lower rotational quantum number for that particular transition. The odd-numbered J transitions are only half as strong as their adjacent even-numbered neighbors and are omitted from this investigation. The lowest-J transitions, S(0) through S(4), have gains that decrease less quickly with altitude and are shown in Figure 8, where the vertical scale has been magnified by a factor of three from that of Figure 7. The integrated gain coefficients over the depth of the atmosphere (from sea level to 100 km) for all these transitions are tabulated in Table 1.

Raman gains for frequencies other than those at the peak [$\delta\nu = 0$ in equation (1)] of the Raman transitions were also calculated. Figure 9 shows the S(8) gain coefficient as a function of altitude for detuning values of 0, 10, 100, and 800 MHz. The integrated (over altitude) gain coefficient for S(8) is plotted versus detuning in Figure 10.

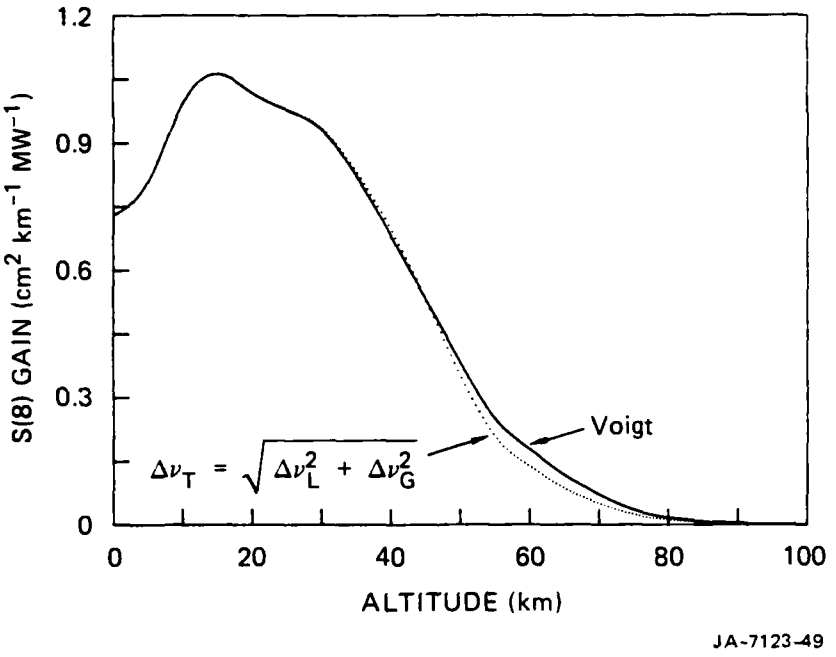

FIGURE 4 RAMAN GAIN COEFFICIENT FOR THE S(8) TRANSITION. The solid curve is the peak, steady-state, plane wave Raman gain coefficient of S(8) in N_2 as a function of altitude in the atmosphere. The dotted curve shows the gain if the approximation, $\Delta\nu_T^2 = \Delta\nu_G^2 + \Delta\nu_L^2$, is used in place of an exact Voigt lineshape calculation ($\Delta\nu_T$, $\Delta\nu_G$, and $\Delta\nu_L$ are the total, Gaussian, and Lorentzian linewidths, respectively).

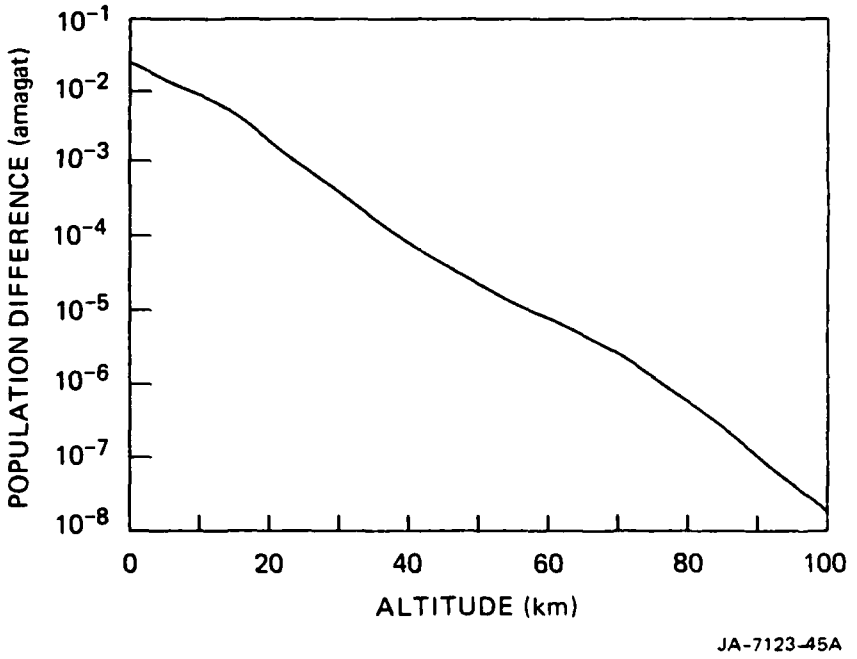

FIGURE 5 POPULATION DIFFERENCE, ΔN, AS A FUNCTION OF ALTITUDE FOR S(8) IN N_2.

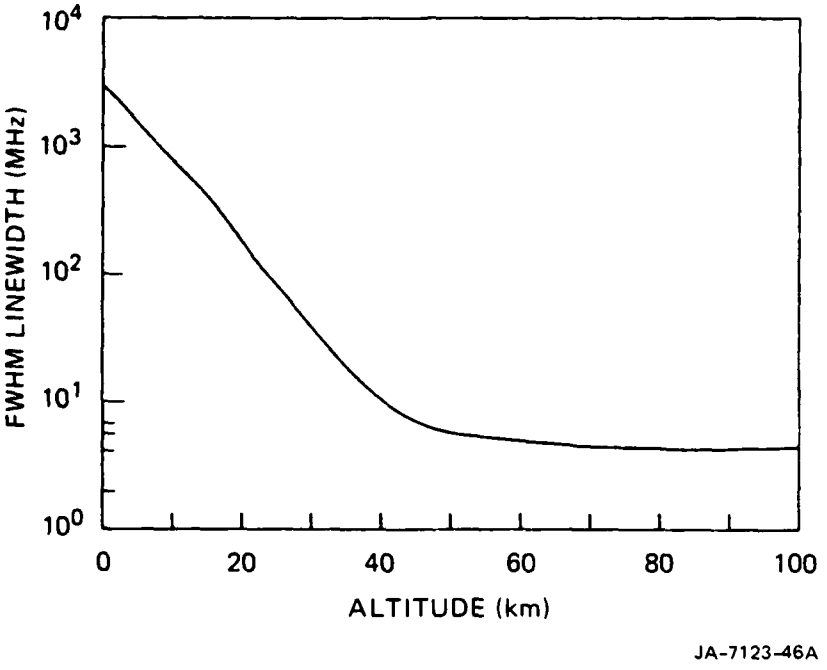

FIGURE 6 RAMAN LINEWIDTH (FWHM) OF VOIGT LINESHAPE AS A FUNCTION OF ALTITUDE FOR S(8) IN N_2.

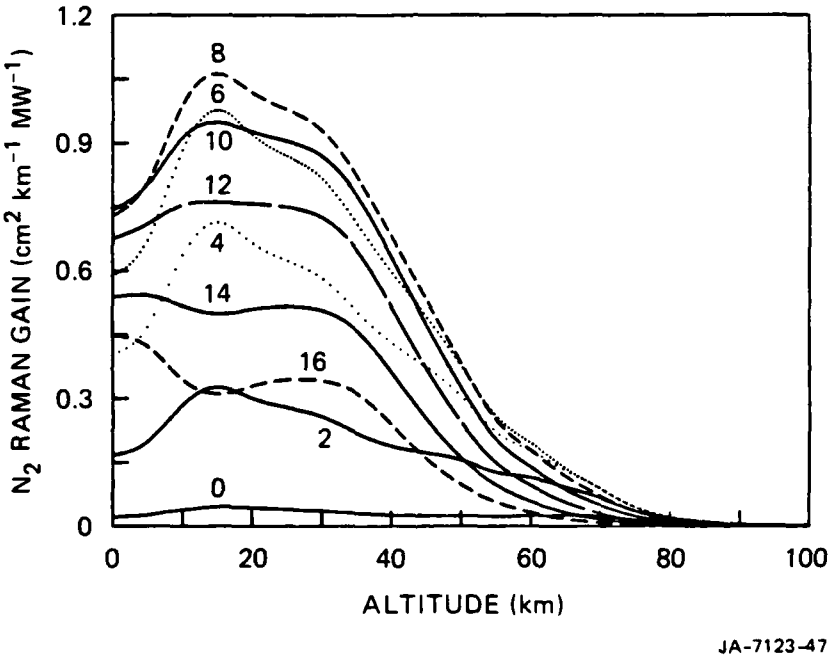

FIGURE 7 PEAK RAMAN GAINS FOR THE STRONGEST STOKES TRANSITIONS IN N_2 AS A FUNCTION OF ALTITUDE.

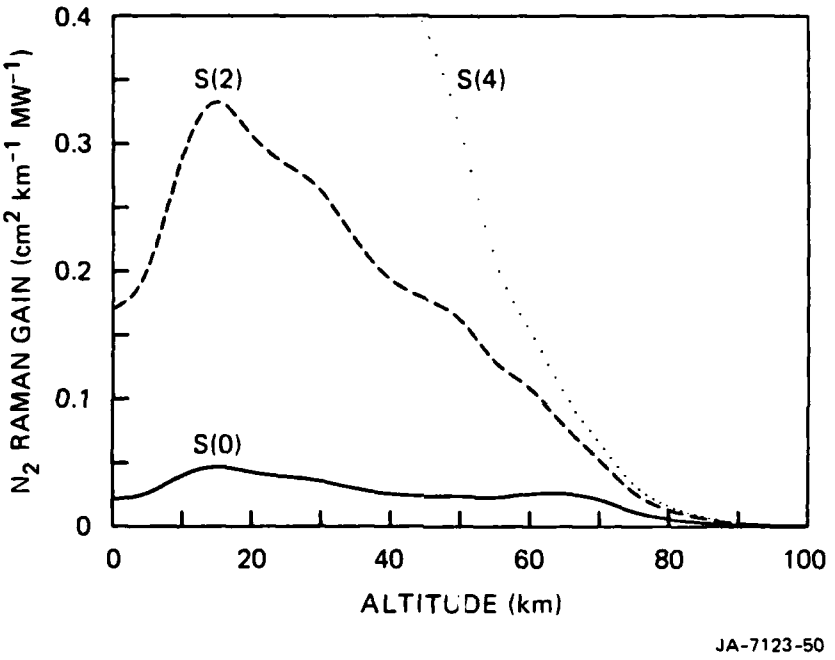

FIGURE 8 PEAK RAMAN GAINS FOR S(0) THROUGH S(4) AS A FUNCTION OF ALTITUDE.

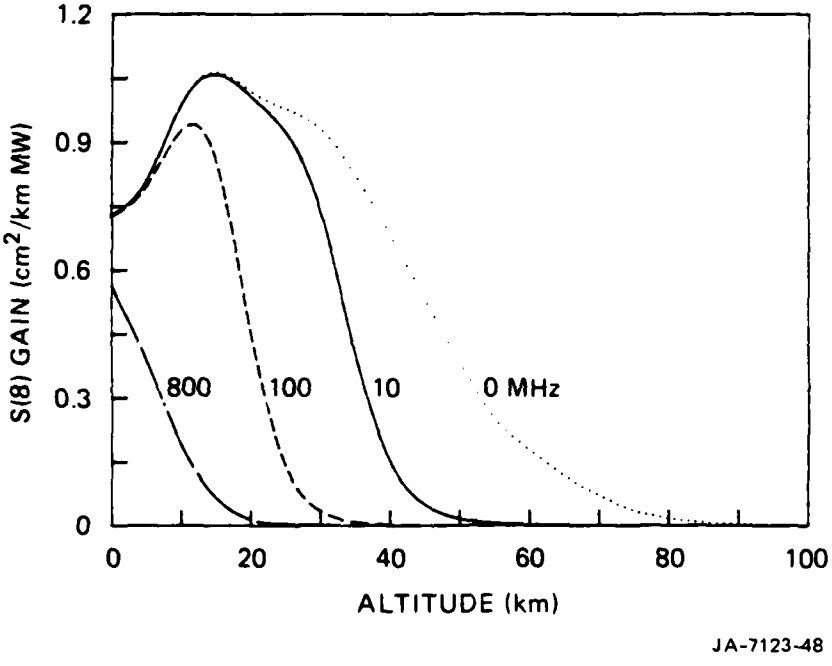

FIGURE 9 S(8) RAMAN GAIN AS A FUNCTION OF ALTITUDE FOR DETUNINGS OF 0, 10, 100, AND 800 MHz FROM THE LINE CENTER.

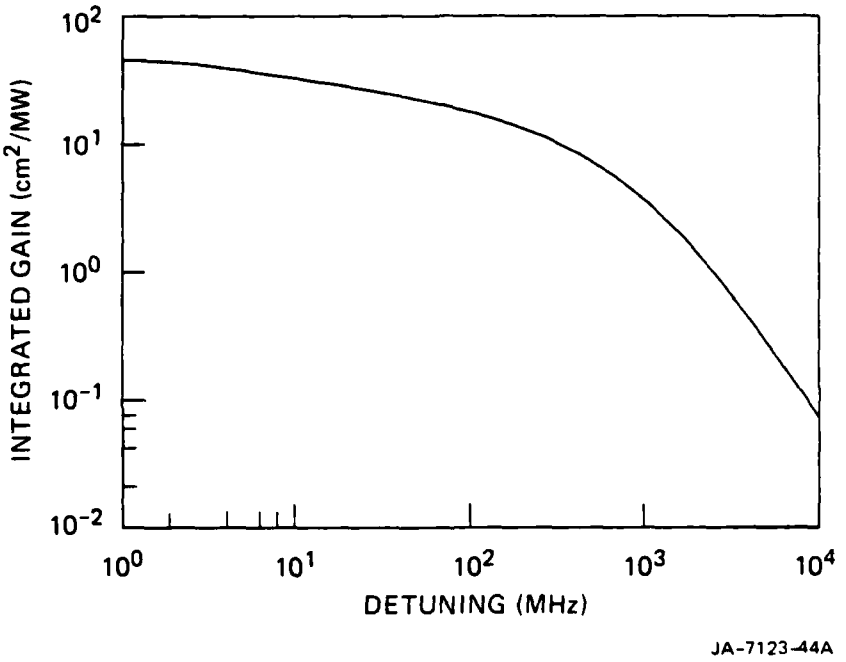

FIGURE 10 INTEGRATED (FROM 0 TO 100 km IN ALTITUDE) RAMAN GAIN FOR S(8) AS A FUNCTION OF DETUNING.

Table 1

PEAK RAMAN GAIN COEFFICIENTS (INTEGRATED FROM SEA LEVEL TO 100 km) FOR STOKES ROTATIONAL TRANSITIONS OF N_2

Transition S(J)	Gain Coefficient ($cm^2\ MW^{-1}$)
0	2.16
2	13.8
4	29.1
6	39.3
8	43.4
10	39.8
12	32.6
14	22.6
16	15.2

B. Seasonal and Laser Linewidth Effects

All the results of Figures 4 through 10 were obtained for the specific temperature profile of Table 3.1 of Reference 1. The effect of atmospheric temperature fluctuations is summarized in the four curves of Figure 11. The Raman gain of S(8), due to seasonal variations of temperature, is shown with two gain profiles for both summer and winter. The curves labeled maximum show the gain for the highest temperatures for that season, whereas those labeled minimum show the gain for the lowest temperatures. Figure 11 shows that maximum variations in the Raman gain due to temperature changes in the atmosphere will be about 10% at all altitudes. The four temperature profiles used in the calculations of Figure 11 are taken from Figure 1.

The last Raman gain parameter discussed here is the laser linewidth. All previous results in this paper were obtained assuming negligible laser linewidths. Appreciable Gaussian laser frequency profiles were also considered. The effect of the laser bandwidth on the gain profiles of S(4) and S(6) is shown in Figures 12 and 13, respectively. The laser linewidths (in MHz) are indicated next to each curve. Integrated gains for all the cases in both of these figures are listed in Table 2. Figures 12 and 13 show that in the absence of phase locking between the pump and Stokes waves,[9-12] large laser bandwidths can effectively reduce the gain length.

C. Voigt Approximation

In this study the Raman lineshape was always modeled as a Voigt function. In this section, a simple approximation (requiring less computation time than an exact Voigt calculation) is presented as an alternative to calculating the Voigt function. This approximation is valid when calculating the peak Raman gain coefficient, but is not applicable for frequencies off the line center.

The procedure uses equation (1) to calculate the peak Raman gain. The lineshape, $f(\delta\nu)$, is approximated as

$$f(\delta\nu=0) = \left[\left(\frac{\Delta\nu_G}{0.9394}\right)^{1.3} + \left(\frac{\Delta\nu_L}{0.6366}\right)^{1.3}\right]^{-0.769} \qquad (4)$$

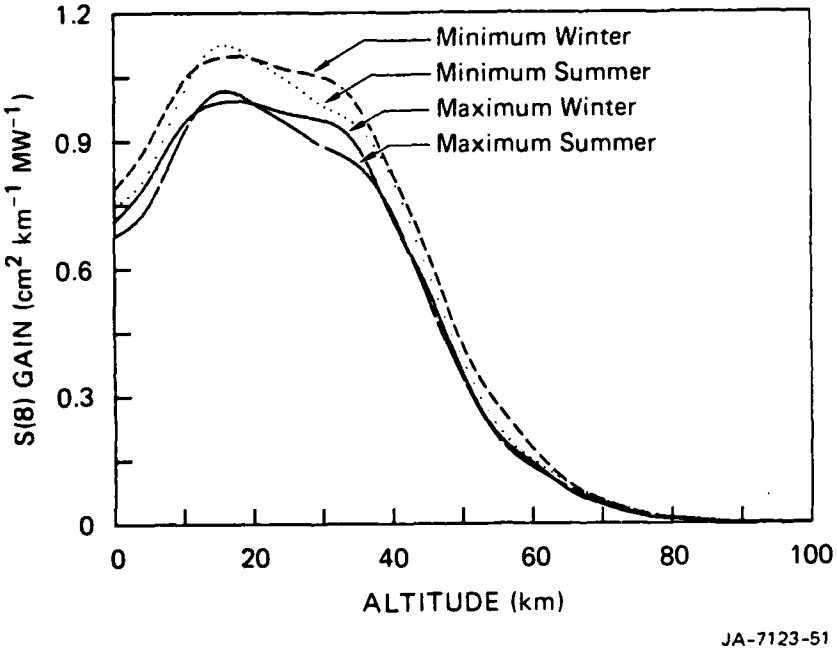

FIGURE 11 S(8) PEAK RAMAN GAIN VARIATIONS FOR MAXIMUM VARIATIONS IN ATMOSPHERIC TEMPERATURES.

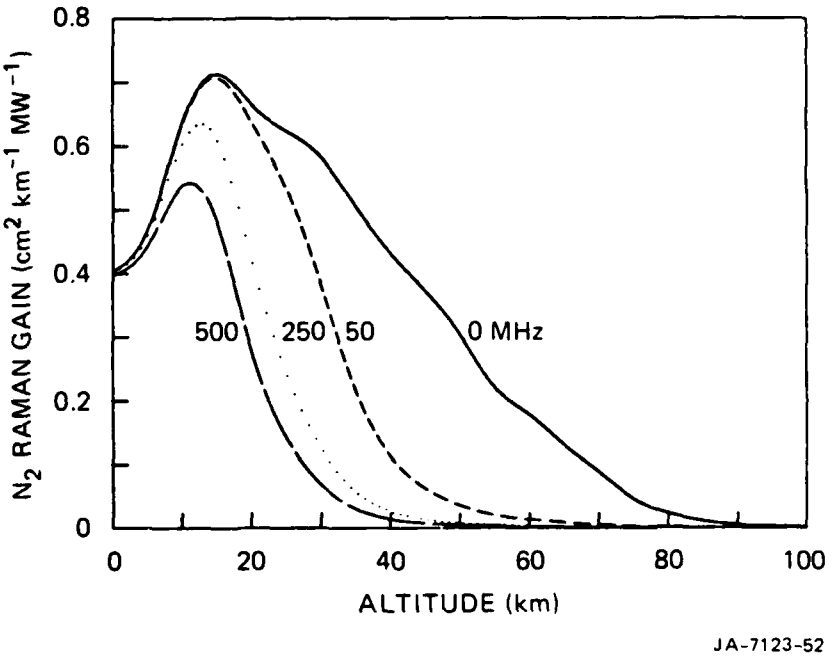

FIGURE 12 S(4) GAIN AS A FUNCTION OF ALTITUDE FOR LASER LINEWIDTHS OF 0, 50, 250, AND 500 MHz. This calculation neglects the phase-locking of the pump and Stokes waves for collinear propagation. If the Stokes wave builds up from noise (not seeded), the steady-state Raman gain will be that of the curve for 0 MHz (assuming dispersion is negligible).

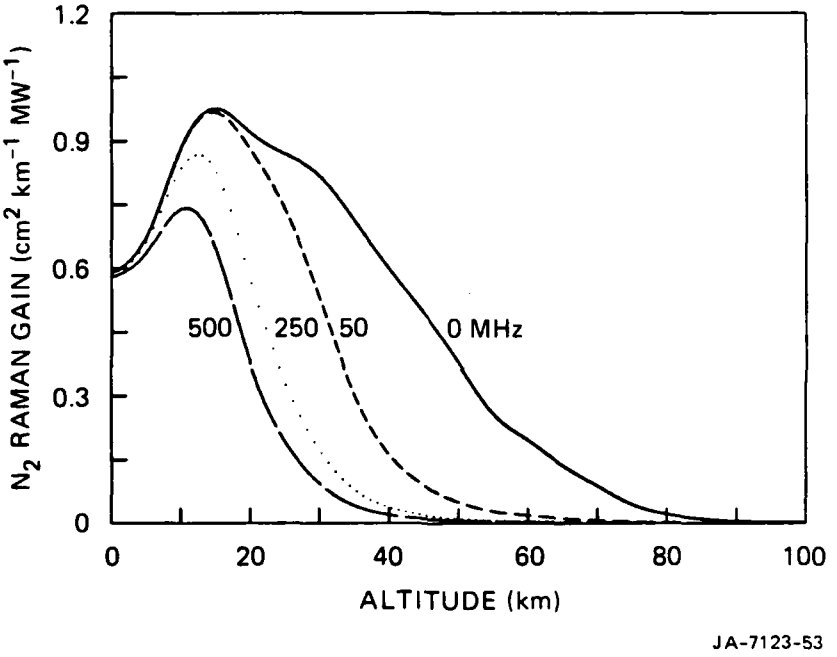

FIGURE 13 S(6) GAIN AS A FUNCTION OF ALTITUDE FOR LASER LINEWIDTHS OF 0, 50, 250, AND 500 MHz. This calculation neglects the phase-locking of the pump and Stokes waves for collinear propagation. If the Stokes wave builds up from noise (not seeded), the steady-state Raman gain will be that of the curve for 0 MHz (assuming dispersion is negligible).

Table 2

Peak Raman gain coefficients (integrated from sea level to 100 km) for various laser linewidths.

Laser Linewidth (MHz)	Gain Coefficients (cm^2 MW^{-1})	
	S(4)	S(6)
0	29.2	39.3
50	18.9	26.5
250	13.0	18.1
500	10.3	14.4

where $\Delta\nu_G$ and $\Delta\nu_L$ are the total Gaussian and Lorentzian FWHM linewidths. The difference between the approximation of equation (4) and an exact Voigt calculation is illustrated in Figure 14, where the Raman gain for both cases is plotted as a function of the ratio of the Lorentzian and Gaussian contributions to the linewidth. The fractional difference of $f(\delta\nu=0)$ for the two methods is also shown, and has a maximum value of about 3%. Results in Figure 14 are obtained with a constant Gaussian FWHM of 5 MHz, corresponding to the Doppler broadening of S(8) at room temperature.

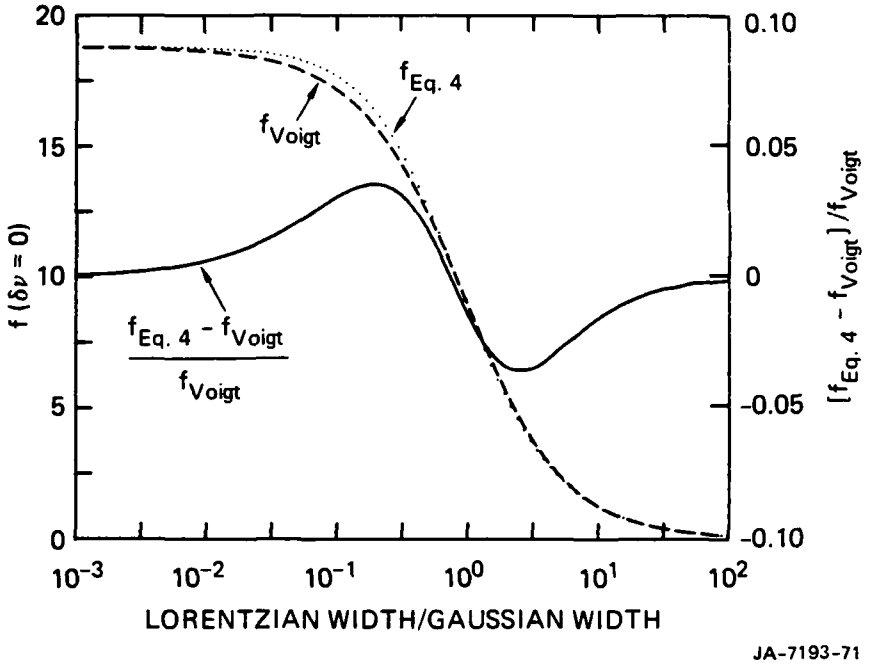

FIGURE 14 COMPARISON OF $f(\delta\nu=0)$ USING THE EXACT VOIGT LINESHAPE (DASHED CURVE) AND THE APPROXIMATION GIVEN BY EQUATION (4) (DOTTED CURVE). The fractional difference (solid curve) is also shown. The variable along the horizontal axis is the ratio of the Lorentzian linewidth to the Gaussian linewidth and the Gaussian FWHM is held constant at 5 MHz.

IV SUMMARY

The Raman gain of the Stokes rotational lines in N_2 has been modeled as a function of altitude for the lower 100 km of the atmosphere. Calculations were completed for the even-J transitions, S(0) through S(16). The strongest lines, S(6) through S(10), have gain coefficients that are approximately constant at 1 cm^2 MW^{-1} km^{-1} over the lower 40 km and then decrease to zero over the 40-80 km region. Effects on the Raman gain are described for seasonal temperature fluctuations in the atmosphere, laser linewidths, and detuning from the line center of the Raman transition.

The uncertainties in the Raman gain coefficients reported here depend on how well the temperature of the gain medium is known. If the temperature is accurately known (e.g., laboratory conditions), the uncertainties in the gain coefficients are limited by the uncertainties in the linewidths and the polarizability anisotropy. Both of these uncertainties are about 1-2%; thus, the gain coefficient uncertainties are about 5%. In the atmosphere, where the temperature is not well known, the uncertainties in the gain coefficients are dominated by temperature uncertainties. Therefore, gain coefficient uncertainties are about 10%, as illustrated in Figure 11.

REFERENCES

1. P. M. Banks and G. Kockarts, Aeronomy, Chapter 3 (Academic Press, New York, 1973).

2. M. A. Henesian, C. D. Swift, and J. R. Murray, "Stimulated Rotational Raman Scattering in Long Air Paths," Opt. Lett. 10, 565 (1985).

3. M. P. Bogaard, A. D. Buckingham, R. K. Pierens, and A. H. White, "Rayliegh Scattering Depolarization Ratio and Molecular Polarizability Anisotropy for Gases," J. C. S. Faraday I 74, 3008 (1978).

4. G. R. Alms, A. K. Burnham, and W. H. Flygare, "Measurement of the Dispersion in Polarizability Anisotropies," J. Chem. Phys. 63, 3321 (1975).

5. C. M. Penny, R. L. St. Peters, and M. Lapp, "Absolute Raman Cross Section for N_2, O_2, and CO_2," J. Opt. Soc. Am. 64, 712 (1974).

6. N. J. Bridge and A. D. Buckingham, "The Polarization of Laser Light Scattered by Gases," Proc. Roy. Soc. (London) A295, 334 (1966).

7. Landolt-Börnstein, Zahlenwerte und Funktionen II. Band, 8. Teil, Optishe Konstanten (Springer-Verlag, Berlin, 1962).

8. K. P. Huber and G. Herzberg, Molecular Spectra and Molecular Structure IV. Constants of Diatomic Molecules, (Van Nostrand Reinhold Company, New York, 1979), p. 420.

9. A. Flusberg, "Stimulated Raman Scattering in the Presence of Strong Dispersion," Opt. Commun. 38, 427 (1981).

10. E. A. Stappaerts, W. H. Long, Jr., and H. Komine, "Gain Enhancement in Raman Amplifiers with Broadband Pumping," Opt. Lett. 5, 4 (1980).

11. W. R. Trutna, Jr., Y. K. Park, and R. L. Byer, "The Dependence of Raman Gain on Pump Laser Bandwidth," IEEE J. Quantum Electron. QE-15, 648 (1979).

12. A. Flusberg, D. Kroff, and C. Duzy, "The Effect of Weak Dispersion on Stimulated Raman Scattering," (to be published).

Appendix A

TEMPERATURE AND WAVELENGTH DEPENDENCE OF THE ROTATIONAL RAMAN GAIN COEFFICIENT IN N_2

G. C. Herring, Mark J. Dyer, and William K. Bischel
Chemical Physics Laboratory
SRI International, Menlo Park, CA 94025

ABSTRACT

The temperature, wavelength and J dependence of the rotational Raman gain coefficient has been determined for the S branch transitions in N_2. First, the temperature dependence (80-300K) of the density-broadening coefficients was measured using stimulated Raman spectroscopy. Second, the wavelength dependence (250-600nm) of the polarizability anisotropy was emperically determined by fitting to the most recent experimental data. These two results were then used to calculate the rotational Raman gain coefficients with accuracies estimated at 5%. At room temperature, the high density limit of the steady-state gain coefficient of the strongest line, S(10), is 4.8×10^{-12} cm/W for a Stokes wavelength of 568 nm.

Accepted for publication in Optics Letters.

MP 85-238
02/06/86

There are many applications, such as laser fusion, that require the propagation of high intensity lasers through the atmosphere. Recently, there has been renewed interest in the nonlinear optical processes that limit the maximum transmitted laser intensity for a given propagation distance. Several different nonlinear effects may be important and some of these were summarized by Zuev[1] in 1982. However, it has only recently been suggested that rotational stimulated Raman scattering (RSRS) in N_2 may ultimately limit the maximum intensity that can be propagated through air if the frequency and divergence of the laser are to remain unchanged. This suggestion is supported by recent experiments[2] at Lawrence Livermore National Laboratory, where RSRS in N_2 was observed when the NOVA fusion laser was propagated through 100 m of air at intensities in the range of a few GW/cm^2.

This observation has reinforced the need for accurate modeling of stimulated Raman scattering in air. Unfortunately, the existing uncertainties[2,3] in the steady-state gain coefficient in N_2 limit the usefulness of any potential model. In particular, no data exist for the temperature dependence of the gain coefficient, an important consideration in any model. In this letter we present new experimental results for the temperature dependence of the Raman gain coefficient for the most important S branch rotational transitions in N_2.

Direct measurement of the gain coefficient requires an accurate measurement of the laser intensity in the interaction region. For low gain Raman systems such as N_2, this is extremely difficult since a focused geometry is usually required to obtain adequate signal strengths. Alternatively, it has been recently experimentally demonstrated[4] that the gain coefficient can be accurately calculated if the lineshape function for the Raman transition and the polarizablility anisotropy are known precisely. We have chosen this

alternative method for determining the rotational Raman gain coefficients in N_2. Using stimulated Raman gain spectroscopy,[5] we have measured the density and temperature dependence of the Raman linewidths for the Stokes branch rotational transitions in N_2. In addition, the relative scattering cross sections were measured for these same rotational lines. Using the results of these measurements and previously published values[6-9] of the polarizability anisotropy, we have calculated the high-density Raman gain in the temperature region 80-300 K for four of these rotational transitions.

For a Lorentzian lineshape function, the peak plane wave, steady-state Raman gain coefficient is[10]

$$g = \frac{2\,\lambda_s^2\,\Delta N}{h\,\nu_s\,\pi\,\Delta\nu}\,\frac{\partial\sigma}{\partial\Omega}\,, \tag{1}$$

where ν_s is the Stokes frequency in hertz, λ_s is the Stokes wavelength in the medium, $\Delta\nu$ is the linewidth (FWHM) in hertz, and ΔN is the population difference, which is equal to $N(J)-[N(J')(2J+1)/(2J'+1)]$. $N(J)$ is the Boltzmann statistical population density in a state with rotational quantum number J. The rotational Raman scattering cross section for incident and scattered waves linearly polarized in the same direction is given by[11]

$$\frac{\partial\sigma}{\partial\Omega} = \frac{2}{15}\left(\frac{2\,\pi\,\nu_s}{c}\right)^4 \frac{(J+1)\,(J+2)}{(2J+1)\,(2J+3)}\,\gamma^2\,, \tag{2}$$

where γ is the polarizability anisotropy. The linewidth in Eq. (1) varies with J, density and temperature, while γ varies with pump laser frequency. Thus, it is necessary to know this parametric dependence in order to accurately calculate the Raman gain.

The experimental setup is a quasi-cw stimulated Raman spectrometer similar to that in Ref. 5. The cw probe laser, which provides 150 mW of power in the interaction region, is a single-mode Kr^+ ion laser operating at 568 nm. The pump laser is a coherent 699-29 single-mode cw ring dye laser that is pulse amplified using a Quanta-Ray PDA-1. At 565 nm, the tunable output of the pump laser consists of 3-mJ, 10-nsec (FWHM) pulses at 10 Hz. The frequency resolution of this system, limited by the linewidth of the pulsed laser, is approximately 100 MHz. A 250-μm-diameter pinhole is used to improve the spatial mode of the pump beam and to verify that the beam does not move when the dye laser is tuned over wavelength intervals of 100 Å. The pump and probe beams were focused and crossed (angle of 1 degree) at the center of a gas sample cell using a 40-cm focal length lens. After the cell, stray pump light was isolated from the probe beam with a second pinhole while an AC-coupled photodiode was used to monitor the probe intensity. The Raman gain signal, which appears as a 10-nsec pulse on the probe laser intensity, is averaged with a gated integrator and stored on disk for later analysis.

Density-broadening coefficients were determined for the S(6), S(8), S(10), and S(12) rotational transitions in N_2. The data were taken at three temperatures (295 K, 195 K, and 80 K) for densities spanning the range 0.01-2 amagat. The results of these measurements are shown in Figure 1 and listed in Table I. The values for the density-broadening coefficient at room temperature are in agreement with ab initio theory[12] (solid line) and are in good agreement with recent linewidth measurements[13] using spontaneous scattering. Simultaneous recording of the Raman signals at two different pressures also allowed the observation of density shifts of the Raman transition frequency. We have determined that the density shifts are less than 150 MHz/amagat for all rotational lines and temperatures studied. These

broadening and shift measurements will be described in greater detail in a future publication.[14]

The ground state polarizability anisotropy is defined as $\gamma = \alpha_{\parallel} - \alpha_{\perp}$ where $(\perp,\parallel)$ indicate the perpendicular and parallel components, respectively, of the polarizability α. We can model the wavelength dependence of γ using an empirical formula[6]

$$\gamma(\nu) = \alpha_{s\parallel}\left(\frac{\nu_{i\parallel}^2}{\nu_{i\parallel}^2 - \nu^2}\right) - \alpha_{s\perp}\left(\frac{\nu_{i\perp}^2}{\nu_{i\perp}^2 - \nu^2}\right), \qquad (3)$$

where ν is the pump laser frequency, $\alpha_{s\perp,\parallel}$ is the static or DC polarizability, and $\nu_{i\perp,\parallel}$ is an effective intermediate state. The $\nu_{i\perp,\parallel}$ were determined first by fitting Eq. (3) to the results of recent <u>ab initio</u> calculations[7] for $\alpha_{\parallel}$ and $\alpha_{\perp}$. The $\alpha_{s\parallel}$ and $\alpha_{s\perp}$ were then obtained by fitting Eq. (3), with $\nu_{i\perp,\parallel}$ fixed, to recent experimental determinations[6,8,9] of $\alpha_{\parallel}$ and $\alpha_{\perp}$ to obtain $\alpha_{s\parallel}$ and $\alpha_{s\perp}$. The N_2 parameters derived using this procedure are: $\nu_{i\parallel} = 1.260 \times 10^5$ cm^{-1}, $\nu_{i\perp} = 1.323 \times 10^5$ cm^{-1}, $\alpha_{s\parallel} = 2.200 \times 10^{-24}$ cm^3, and $\alpha_{s\perp} = 1.507 \times 10^{-24}$ cm^3.

In Fig. 2, the wavelength dependence of $\gamma(\nu)$, from Eq. (3), is shown along with several experimental values. We have used data from only Refs. 6, 8 and 9 to determine the $\alpha_{s\perp,\parallel}$ because these measurements have substantially smaller uncertainties than the other Refs. cited in Fig. 2. Eqs. 2 and 3 yield cross sections that are in agreement with direct measurements.[15,16]

In N_2, the J dependence of the polarizability anisotropy, γ, is negligible[17,18] for $J \lesssim 20$. We have verified this conclusion by determining the relative cross sections from our stimulated Raman lineshape measurements. Thus we have used Eq. (3) to determine the polarizability anisotropy for all transitions studied in this letter.

The reliability of Eq. (3) can be checked by using the parameters $\alpha_{s\perp,\parallel}$ and $\nu_{i\perp,\parallel}$ to calculate the index of refraction, n; the result can then be compared with experimental data. The expression for n-1 is

$$\frac{2}{3}(n-1) \approx \frac{n^2-1}{n^2+2} = \frac{4\pi N}{9}\left[\alpha_{s\perp}\left(\frac{2\nu_{i\perp}^2}{\nu_{i\perp}^2-\nu^2}\right)+\alpha_{s\parallel}\left(\frac{\nu_{i\parallel}^2}{\nu_{i\parallel}^2-\nu^2}\right)\right], \qquad (4)$$

where N is the density. Over the wavelength range 250-600 nm, Eq. (4) agrees with experimental data[19] to better than 0.5%, verifying a high accuracy for $\gamma(\nu)$ of Eq. (3).

We have used Eqs. 1-3 and our linewidth data to calculate the Raman gain coefficient for the rotational transitions as a function of temperature in the limit where density broadening is the dominant contributor to the linewidth. For N_2, this high-density limit corresponds to densities greater than 0.01 amagat. The results are summarized in Table I, while the temperature dependence is illustrated in Figure 3. These results were obtained by assuming the rotational linewidths are linear with temperature and the polarizability anisotropy is constant with J.

The accuracy of the gain coefficients reported here is limited by the uncertainties in the linewidths and the polarizability anisotropy. Our linewidth measurements have uncertainties of 2% (one standard deviation) as given by the linear fits used to determine the broadening coefficients.[14] The uncertainty in the polarizability anisotropy was estimated to be 1.5% from the differences in the results of different investigators. Thus the accuracy of the gain coefficients reported here is approximately 5%.

We can compare the pure N_2 gain coefficients reported here with the air coefficients reported by Henesian et al.,[2] since we have also measured[14] the foriegn gas broadening coefficients of O_2. After correcting for N_2 and O_2

densities, λ_s, and the wavelength dependence of the polarizability anistropy (Eq. 3), we obtain a N_2 gain coefficient of 2.0×10^{-12} cm/W for one atmosphere (80%/20% mixture of N_2/O_2) at $\lambda_s = 1.07$ μm. This is 25% smaller than the value of Henesian et al.[2], but consistant with their error bar of a few tens of per cent.

In conclusion, we have made linewidth and cross section measurements that will facilitate the modeling of stimulated rotational Raman scattering in N_2. Linewidths are linear with density for densities from 0.01 to 2.0 amagat and are also linear with temperature for temperatures from 80 K to 300 K. Within the accuracy (± 5%) of our relative measurements, the polarizability anisotropy was found to be independent of J for S(2) through S(16). The new linewidth data presented here can now be used to accurately (±5%) predict the rotational Raman gain over a wide range of temperatures and densities in N_2.

In addition to rotational Raman scattering, vibrational Raman scattering is appreciable for the intensities used in this work. A room temperature study has already been reported,[20] and future work in this area should include an investigation of the temperature dependence of the gain for the vibrational transition in N_2.

This work was supported by the Defense Advanced Research Projects Agency under Contract N00014-84-C-0256, through the Office of Naval Research.

REFERENCES

1. V. E. Zuev, Laser Beams in the Atmosphere (Consultants Bureau, New York, 1982) pp. 243-314.

2. M. Henesian, C. Swift, J. R. Murray, "Stimulated Rotational Raman Scattering in Long Air Paths," Opt. Lett. 10, 565 (1985).

3. V. S. Averbakh, A. I. Makarov, and V. I.Talanov, "Stimulated Raman Scattering on Rotational Vibrational Transitions in Nitrogen Gas," Sov. J. Quantum Electron.,8, 472 (1978).

4. William K. Bischel and Mark J. Dyer, "Wavelength Dependence of the Absolute Raman Gain Coefficient for the Q(1) Transition in H_2" (submitted for publication).

5. P. Esherick and A. Owyoung, "High Resolution Stimulated Raman Spectroscopy," in Advances in Infrared and Raman Spectroscopy, edited by R.J.H. Clark and R. E. Hestor (Heyden and Son Ltd., London, 1983).

6. G. R. Alms, A. K. Burnham, and W. H. Flygare, "Measurement of the Dispersion in Polarizability Anisotropies," J. Chem. Phys., 63, 3321 (1975).

7. P. W. Langhoff, "Moment Theory Bounds for the Second-Order Optical Properties of Atoms and Molecules," J. Chem. Phys. 57, 2604 (1972).

8. Martin P. Bogaard, A. David Buckingham, Raymond K. Pierens, and Allan H. White, "Rayleigh Scattering Depolarization Ratio and Molecular Polatizability Anisotropy for Gases," J.C.S. Faraday I 74, 3008 (1978).

9. N. J. Bridge and A. D. Buckingham, "The Polarization of Laser Light Scattered by Gases," Proc. Roy. Soc. (London) A295, 334 (1966).

10. J. R. Murray, J. Goldhar, D. Eimerl, and A. Szoke, "Raman Pulse Compression of Excimer Lasers for Application to Laser Fusion," IEEE J. Quantum Electron. QE-15, 342 (1979).

11. D. A. Long, Raman Spectroscopy (McGraw-Hill, London, 1977).

12. D. Robert and J. Bonomy, "Short Range Force Effects in Semiclassical Molecular Line Broadening Calculations," J. Phys. (Paris) 40, 923 (1978).

13. H.G.M. Edwards, D. A. Long, and S. W. Webb, "Self- and Foreign-Gas Broadening of the Pure Rotational Raman Line of Oxygen and Nitrogen," Proceeding of IXth International Conference on Raman Spectroscopy (1984).

14. G. C. Herring, Mark J. Dyer, and William K. Bischel, "Temperature and Density Dependence of the Linewidths and Lineshifts of the Rotational Raman Lines in N_2 and H_2," (submitted to Phys. Rev. A).

15. C. M. Penny, R. L. St. Peters, and M. Lapp, "Absolute Rotational Raman Cross Sections for N_2, O_2, and CO_2," J. Opt. Soc. Am. 64, 712 (1974).

16. Wyanne R. Fenner, Howard A. Hyatt, John M. Kellam, and S.P.S. Porto, "Raman Cross Section of Some Simple Gases," J. Opt. Soc. Am. 63, 73 (1973); corrected by data in J. Opt. Soc. Am. 63, 1604 (1973).

17. Chamnong Asawaroengchai and Gerd M. Rosenblatt, "Rotational Raman Intensities and the Measured Change with Internuclear Distance of the Polarizability Anisotropy of H_2, D_2, N_2, O_2, and CO," J. Chem. Phys. 72, 2664 (1979).

18. Hiro-o Hamaguchi, A. D. Buckingham, and W. J. Jones, "Determination of the Polarizability Anisotropy in Diatomic Molecules II. The Hydrogen and Nitrogen Molecules," Molecular Physics, 43, 1311 (1981).

19. Landolt-Börnstein, Zahlenwerte und Funktionen II. Band, 8. Teil, Optishe Konstanten (Springer - Verlag, Berlin, 1962).

20. G. J. Rosasco, W. Lempert, and W. S. Hurst, "Line Interference Effects in the Vibrational Q-Branch Spectra of N_2 and CO," Chem. Phys. Lett. 97, 435 (1983)

FIGURE CAPTIONS

Figure 1. Measured temperature dependence of the density-broadening coefficient for Stokes branch rotational Raman transitions in N_2. The solid line indicates the most recent room temperature *ab initio* calculations given in Ref. 12.

Figure 2. Wavelength dependence of the N_2 polarizability anisotropy. Solid line is given by Eq. (3), which was derived with a fit to the data of Refs. 6, 8, and 9. Data of Refs. 2 and 15 were not used in the fit, but are shown for comparison.

Figure 3. Temperature dependence of the plane wave, steady-state Raman gain in N_2 calculated from Eq. 1 for the high-density limit ($\rho > .01$ amagat). The pump and Stokes polarizations are linear and parallel.

Table I. Temperature dependence of rotational Raman linewidths, fractional population differences, and gain coefficients for S branch in N_2 (λ_s = 568 nm).

S Branch Transition S(J)	Fractional Population Difference	Broadening Coefficient (MHz/amagat)	Gain Coefficient (10^{-12} cm/W)
	T = 295 K		
6	.0282	3570	3.6
8	.0337	3280	4.6
10	.0335	3070	4.8
12	.0289	2870	4.3
	T = 195 K		
6	.0485	3070	7.2
8	.0491	2860	7.6
10	.0399	2660	6.5
12	.0271	2340	4.9
	T = 80 K		
6	.0897	2530	16.1
8	.0452	2120	9.3
10	.0156	1950	3.4
12	.00378	1690	0.91

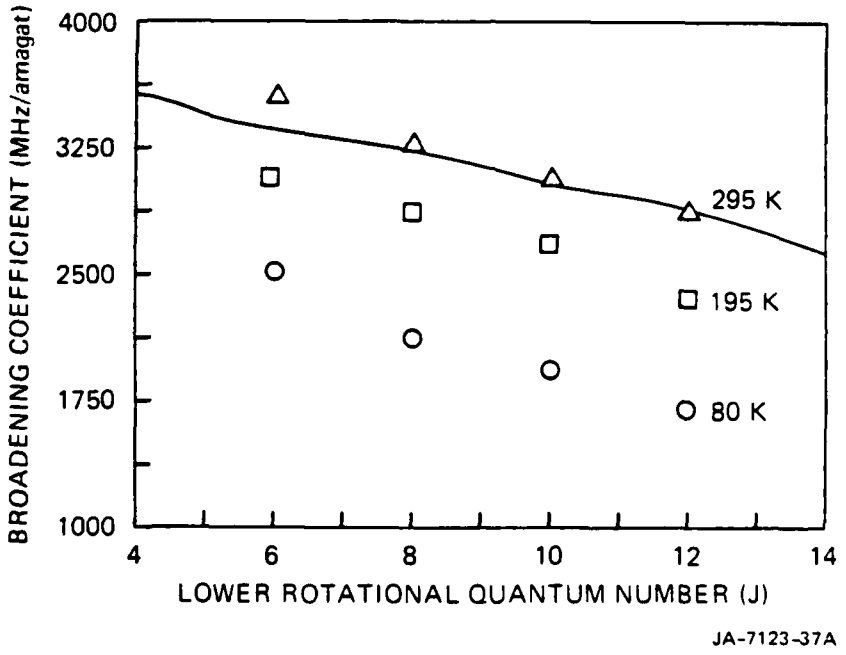
BROADENING COEFFICIENT (MHz/amagat)
4000
3250
2500
1750
1000
4
6
8
10
12
14
LOWER ROTATIONAL QUANTUM NUMBER (J)
295 K
195 K
80 K
JA-7123-37A

FIGURE 1

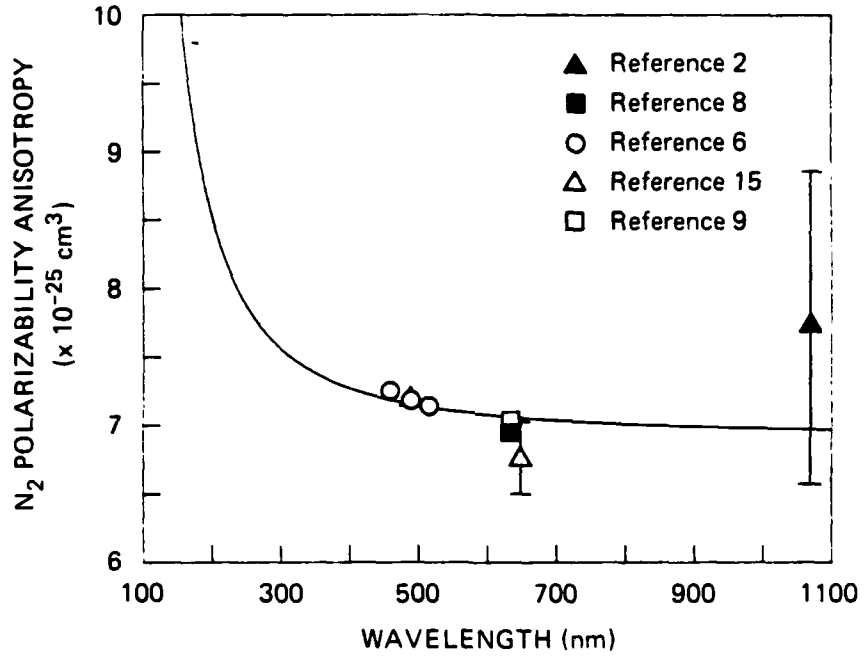
10
9
8
7
6
100
300
500
700
900
1100
WAVELENGTH (nm)
N_2 POLARIZABILITY ANISOTROPY
(x 10^{-25} cm^3)
Reference 2
Reference 8
Reference 6
Reference 15
Reference 9
JA-7123-68A

FIGURE 2

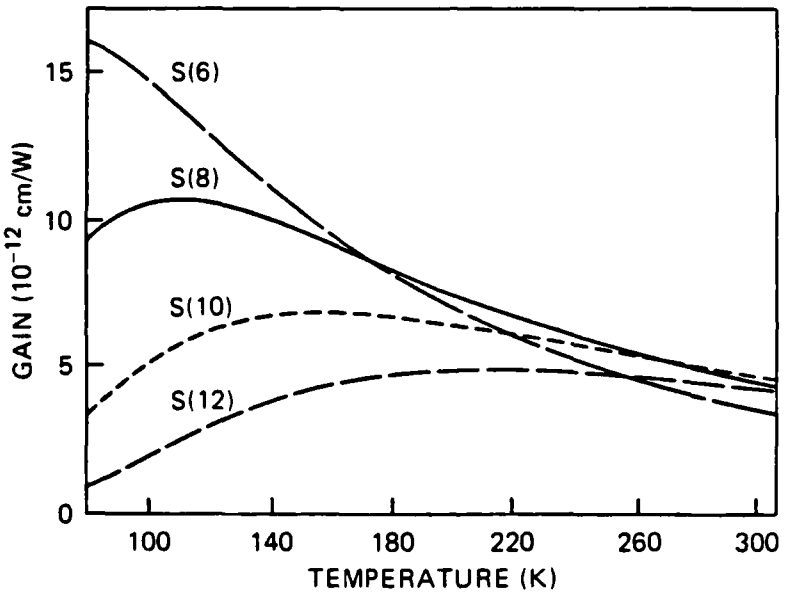
15
10
5
0
S(6)
S(8)
S(10)
S(12)
GAIN (10^{-12} cm/W)
100
140
180
220
260
300
TEMPERATURE (K)
JA-7123-35A

FIGURE 3

Appendix B

TEMPERATURE AND DENSITY DEPENDENCE OF THE LINEWIDTHS AND LINESHIFTS OF THE ROTATIONAL RAMAN LINES IN N_2 AND H_2

G. C. Herring, Mark J. Dyer, and William K. Bischel
Chemical Physics Laboratory
SRI International
Menlo Park, CA 94025

ABSTRACT

The temperature and density dependence of the rotational Raman linewidths and lineshifts for the diatomic molecules N_2 and H_2 has been measured using stimulated Raman gain spectroscopy. Room temperature results for the density broadening coefficients, B, in N_2 are compared with *ab initio* calculations, while the low temperature (80 K and 195 K) results are the first to be reported. Values of γ in the relation, $B \propto T^{\gamma}$, were determined from fits to the data for self-broadening in N_2 yielding $0.25 < \gamma < 0.39$. Foreign-gas (O_2) broadening coefficients for the N_2 transitions were also measured and found to be 10-15% smaller than the self-broadening coefficients. Our linewidth and lineshift results for H_2 are in general agreement with previous measurements.

Accepted for publication in Physical Review A.

MP 85-247
1/23/86

I. INTRODUCTION

Observation[1] of stimulated rotational Raman scattering in air with the NOVA laser at Lawerence Livermore National Laboratory has generated interest in the modeling of the Raman gain in N_2. Accurate knowledge of the Raman linewidths is necessary[2] for any useful model because the peak Raman gain is inversely proportional to the linewidth. Results of previous studies[3-7] of the room temperature rotational Raman linewidths in N_2 typically differ by 30%, while results at other temperatures have not been reported. The main purpose of this work is to measure the temperature dependence of the linewidths and lineshifts for the rotational Raman transitions (S-branch) in N_2.

This work differs from previous measurements of rotational Raman linewidths[3-7] in three aspects. First, we have measured the temperature dependence of the line broadening over the range 80-300 K. Previous work in N_2 has been only for room temperature. Second, the densities, used in this work (0.01-2.0 amagat) are two orders of magnitude lower than those (1.0-100 amagat) used in previous measurements. Complications due to overlapping of adjacent lines are eliminated by working at lower densities where the Raman lines are typically separated by 100 linewidths. Finally, all previous measurements have used spontaneous Raman scattering, whereas we have used stimulated Raman scattering, which has a frequency resolution several orders of magnitude higher than its spontaneous counterpart.

This paper reports experimental results for line broadening and lineshift coefficients for Stokes rotational Raman transitions in N_2 and H_2. Results are presented for the even J transitions, S(2) through S(16), at temperatures of 80 K, 195 K, and 295 K in N_2 and for S(0) and S(1) at temperatures of 80 K and 295 K in H_2. The foreign gas (O_2) broadening and shifts of the four

strongest N_2 transitions have also been measured at 195 K and 295 K. The room temperature broadening coefficients in N_2 are compared with ab initio calculations, whereas the low temperature N_2 self-broadening and the O_2 foreign gas results are the first to be reported. The present temperature dependence of N_2 is compared to that found in studies of CO and CO_2. Finally the present H_2 results are compared with previous measurements.

II. EXPERIMENTAL

A. Apparatus

An overview of the experimental setup is shown in Fig. 1. This quasi-cw stimulated Raman spectrometer is similar to that developed by Esherick and Owyoung[8] and consists of a cw probe laser; a tunable, pulsed pump laser; a pair of gas (sample and reference) cells; and fast photodiodes to detect the induced Raman gain on the probe beams.

The probe laser is a Kr^+-ion laser, operating at 568 nm and forced into single-mode operation with the insertion of a temperature-stabilized etalon into the cavity. This laser has a time-averaged linewidth less than 30 MHz. The probe beam was split into two equal intensity beams so that Raman signals could be simultaneously obtained from two separate gas samples. After passing through their respective sample cells, both of the cw probe beams were chopped at 10 Hz with a mechanical chopper (not shown in Fig. 1). This resulted in 170 μs square-wave pulses that were incident on the photodiodes. Chopping of the probe increases the saturation intensity for the photodiodes. The average power of the probe beams was 150 mW in both the sample and reference cells.

The pump laser was a tunable, single-mode (1-MHz linewidth) cw dye laser that was pulse amplified using a Quanta-Ray PDA-1. The cw dye laser input to the PDA-1 was typically 400 mW. The PDA-1 was pumped with the 532-nm output (130 mJ per pulse) from a frequency doubled YAG laser. At 565 nm, the tunable output of the PDA-1 consisted of 2-mJ, 10-nsec (FWHM) pulses at 10 Hz. The linewidth of the pump laser was 100 MHz, about a factor of two larger than the Fourier transform limit for a 10-ns pulse. Peak pump intensities at the focal planes were estimated to be 5 GW/cm^2 in the sample cell and 70% of that in the reference cell.

The pump and probe beams were mode-matched and then were focused and crossed in the gas cells using 40-cm focal length lenses. The crossing angle was 1.0 degree in both of the cells. A series of diaphrams placed around the probe beams was used to eliminate scattered pump light. Both probe beams were monitored with reversed biased photodiodes that had rise times of less than 1.0 ns, and were terminated with 50-Ω resistors. The total probe power incident on the photodiodes during the 170-μs probe laser pulses was 10 mW. Capacitors (300 pf) were used to block the 170-μs pulses and to pass the 10-ns Raman signals. These signals were amplified by a factor of 100 and then averaged with gated integrators. Output time constants for the integrators and total scan times were usually 0.5 s and 4 min, respectively. Occasionally, for weak transitions, time constants and scan times were increased to 2.5 s and 10 min, respectively. After the pump beam exited the reference cell, it was also monitored with a third photodiode. This signal was used to normalize the two Raman signals for slow pump power variations during the scans.

The sample cell was constructed by attaching a pair of 3.0-cm-diameter brewster window extensions to a drilled-out 10 cm^3 cube of aluminum. One face

of the aluminum cube is in contact with a second reservoir that can be filled with either liquid N_2 or an acetone dry-ice bath. The cooled sample cell was insulated with a vacuum, and the temperature was monitored with a thermocouple that was imbedded in the aluminum cube. The reference gas cell was kept at room temperature and a pressure of 10 torr for N_2 scans and 200 torr for most of the H_2 scans.

The temperature dependence of the linewidths and lineshifts was measured by taking measurements at three temperatures: 80 K, 195 K, and 295 K. At each temperature the lineshape was recorded for several densities over the range 0.01-2.0 amagat. For the low temperature runs, there was a time period ranging from a few to 15 minutes between scans with different densities, so that any gas added between scans always had sufficient time to come to thermal equilibrium with the cell. For each set of runs at constant temperature, the density was randomly changed rather than constantly adding or eliminating gas from the sample cell for each succeeding run.

The pressure in the experimental cells was measured using a 10,000-torr MKS Baratron gauge, and the temperature was measured using a Chromel-Alumel thermocouple gauge referenced to 273 K. The density for both N_2 and H_2 was calculated using the perfect gas law since the density calculated using the second virial coefficient[9] deviates from this calculation by less than 1% at the densities and temperatures used in these experiments.

B. Data Analysis

Since the laser linewidth was comparable to the low density Raman linewidth, it was important to account for this instrumental width in the data analysis. Although the pump laser frequency profile was not directly measured, it was indirectly determined by scanning the laser over a narrow

Raman line (e.g., S(0) in H_2 at 5 torr). This transition has negligible (1 MHz) collisional broadening compared to 100 MHz of Doppler broadening. The profile for this transition was found to fit extremely well to a pure Gaussian. Since the convolution of two Gaussians results in another Gaussian, we concluded that the pump laser profile could be approximated as a Gaussian. Fitting Voigt profiles to low density, narrow N_2 lineprofiles with known Doppler and Lorentzian contributions confirmed this conclusion. The probe laser linewidth was assumed to be negligible when convolved with the pump linewidth; thus all the data presented here were analyzed assuming a Gaussian profile for the instrumental width.

The fitting procedure used to determine the Lorentzian portion of the lineshapes was different for the N_2 and H_2 data. We first describe the fitting procedure for the N_2 transition. For high densities in N_2, Doppler broadening (10 MHz) and the laser linewidth (100 MHz) can be neglected. Thus sample cell lineshapes for high densities were fit to pure Lorentzians to get a first approximation to the Lorentzian width. The low density reference cell data were then fit to Voigt lineshapes with a fixed Lorentzian (determined from the high density fits) and variable Gaussian components. This Gaussian component, representing the pump laser profile for that particular scan, was then used in a final Voigt fit to the sample cell profile. Any fluctuations in the pump laser linewidth from scan to scan were accounted for with this procedure. The change in Lorentzian linewidth determined from the first Lorentzian fit and the final Voigt fit was typically a few percent and further iterations were not necessary.

For the H_2 transitions studied, experimental constraints did not allow the density in the cell to be larger than 3 amagat. Therefore the approximate density broadening coefficient could not be determined from the high density

data. Hence, the above procedure was not applicable. Instead, all of the H_2 lineshapes were fit to Voigt profiles with freely adjustable Lorentzian and Gaussian components.

III. RESULTS

A. Line Broadening in N_2

An example of the S(10) Raman profile in N_2 at 195 K is shown in Fig 2. The narrower profile was taken at 10 torr and the wider profile was taken at 400 torr. Individual dots represent the data, and the sol d line represents the fit for a Voigt lineshape, which is dominated by its Lorentzian component for the 400-torr data. A slight asymmetry is observable in the data of Fig. 2 and was characteristic of most of the N_2 data obtained. An asymmetry of this magnitude will not have an appreciable effect on the linewidth determinations, but could produce significant systematic errors in the lineshift determinations because the lineshifts are so small. This asymmetry is discussed later in Section C.

For densities larger than 0.004 amagat (~ 3 torr at 298 K), the rotational Raman lines of N_2 are collision broadened giving a Lorentzian lineshape function. Hence, the linewidth will be a linear function of density. We have therefore taken the Lorentzian component resulting from the data fitting procedure described in the previous section and determined the density broadening coefficients B for each temperature studied by fitting the linewidths to a straight line. The data and the linear fit (solid line) for the S(10) transition are given in Fig. 3 for temperatures of 298, 195, and 80 K. Individual points indicate the data, and the solid lines represent the least squares fits. Uncertainties (one standard deviation) for the broadening coefficients determined from the fits in Fig. 3 are 1-2%.

Table I summarizes all of the N_2 self-broadening coefficients measured in this study. These values are graphically illustrated in Fig. 4 as a function of rotational quantum number. Odd J transitions in N_2 were not studied. For

S(4) through S(12), the specified uncertainties are one standard deviation for the least squares fit. For S(0), S(2), S(14), and S(16), data were obtained at only one density, and the uncertainties shown for these transitions represent the error in the linewidth determination of a single line profile.

Earlier room temperature measurements by different authors[3,6,7] have shown considerable disagreement (30%). Table III compares these earlier results with our present results. It can be seen that the three earlier studies show significant differences, while our current measurement is consistant with that of Ref. 7. The results of the three previous studies that are shown in Table III were obtained at densities where adjacent lines appreciably overlapped with one another, whereas the present results were obtained at densities where there was no overlapping. We postulate that the differences in the experimental results of the previous studies given in Table III are due to systematic errors arising from the overlapping of adjacent lines.

Theoretical calculations of the collision broadened linewidth Raman have been performed by Grey and Van Kranendonk,[10] Srivastava and Zaidi,[11] and Robert and Bonomy.[12] The difference in these three approaches is in the treatment of the short range intermolecular interactions. The results of these different approaches are compared with our measurements in Fig. 5, where the room temperature broadening coefficients are shown as a function of rotational quantum number J. We also show the experimental values of Jammu et al.[3] for comparison. It should be noted that Srivastava and Zaidi[11] have used an adjustable parameter to obtain their fit to the data of Jammu et. al.,[3] whereas the calculations of Grey and Van Kranendonk[10] and Robert Bonomy[12] do not use any adjustable parameters. Fig. 5 shows the <u>ab initio</u> calculations of Robert and Bonamy[12] to be in the best agreement with our measurements.

Previous to this work, only atomic foreign-gas (He and Ar) broadening of

the N_2 transitions had been investigated.[3] We have also measured diatomic foreign-gas (O_2) broadening coefficients at 195 K and 295 K for the four strongest N_2 transitions. Our O_2 results in Table II show that the foreign-gas broadening by O_2 is typically 85-90% of the self-broadening at both temperatures. Thus the foreign-gas broadening by O_2 is approximately 30% larger than the foreign-gas broadening by the atomic gases.[3]

B. Line Broadening in H_2

The Raman linewidth for H_2 has a much more complex density dependence than that for N_2. This results mainly from the fact that the H_2 density broadening coefficient is approximately a factor of 30 smaller than the N_2 broadening coefficient, and thus Dicke[13] or collisional narrowing of the Raman linewidth can be observed[14,15] in the low density regime if the resolution is high enough. A summary of the relevant collisional processes that contribute to the linewidth at various densities is given in Ref. 14.

For densities above a certain cutoff density (ρ_c defined below), the Raman linshape function is Lorentzian with a FWHM linewidth $\Delta\nu$ that can be expressed as

$$\Delta\nu = A/\rho + B\rho \qquad (1)$$

where A(MHz amagat) is a coefficient proportional to the self-diffusion coefficient $D_o(cm^2\ amagat\ sec^{-1})$. For forward scattering,[14] A is equal to

$$A = 4\pi^2 \nu_R^2 D_o \qquad (2)$$

where ν_R is the Raman transition frequency in cm^{-1}.

This model is known as the diffusion model of the Raman linewidth and it diverges as the density approaches zero. There is a cutoff density, ρ_c, at which this model predicts a linewidth that is 10% larger than that predicted by the "hard collision" lineshape theory.[14] We have previously determined that

$$\rho_c = 3.33\ A/\Delta\nu_D \qquad (3)$$

where $\Delta\nu_D$(MHz) is the FWHM Doppler width of the Raman transition given by (forward scattering)

$$\Delta\nu_D = 7.15\times10^{-7}\ \nu_R\ (T/m)^{1/2} \qquad (4)$$

where ν_R is in MHz, T is the temperature in K and m is the mass in amu. For densities larger than ρ_c, the lineshape is Lorentzian and the widths can be effectively modelled using Eq. 1.

For example, the experimental data set for the S(1) transition at 298 K is given in Fig. 6. From the Voigt fit, we determine both the Lorentzian and Gaussian contributions to the experimental linewidth. Since the Raman lineshape is Lorentzian for all densities shown in Fig. 6, the Gaussian contribution is due to the spectral width of the pulsed dye laser. The Lorentzian and Gaussian contributions to the linewidth are plotted in Fig. 6, where we see that the Gaussian contribution is approximately constant (between

80-100 MHz) while the Lorentzian contribution varies approximately linear in density.

Unfortunately, the 100 MHz resolution of our current laser sytem does not allow the Dicke narrowing of the H_2 rotational Raman linewidth to be resolved with any precision. We have therefore chosen a fitting procedure that uses D_o determined from our previous study[14] to calculate A from Eq. 2. The Lorentzian component of the experimental linewidth for densities larger than ρ_c is then fit to Eq. 1 with one free parameter, B. The parameters used in this fitting procedure are given in Table IV.

The density broadening coefficients B determined using this procedure are given in Table V, where the uncertainties shown are one standard deviation for the one parameter linear least squares fit. This fit is illustrated by the solid line in Fig. 6 for the S(1) transition. The maximum correction to the linewidth due to including the collisional narrowing term in Eq. 1 is on the order of 5-10%.

We have also included in Table V data from the previous work of Van Den Hout et. al.[16] and Cooper, May, and Gupta.[18] There are small discrepancies with the results of Refs. 16 and 18. Some of these differences could be due to small errors that arise in our estimate of A for these rotational transitions. We emphasize that the N_2 results of Section III.B are free of this problem since Dicke narrowing is negligible.

C. Line Shifts in N_2 and H_2

In all of the above cases for which density broadening measurements were reported, we have also made density lineshift measurements. In all cases the lineshifts were only a few percent of the linewidth, and hence any asymmetries in the lineshapes need to be carefully analyzed.

The asymmetry in Fig. 2 is typical of that observed in our data for the higher density N_2 data. The lower density N_2 data contained an asymmetry that occurred only further out in the wing of the spectral profiles. About 80% of the total number of line profiles at all densities and temperatures exhibited this small asymmetry, where the data were slightly larger than the symmetric fit on the high frequency side of the line. Roughly 20% of the line profiles were symmetric and only rarely did the asymmetry appear such that the data were smaller than the fit on the high frequency side. It was determined that this asymmetry was not due to the saturation of the detection system by either the probe beam or the Raman signal. By scanning the dye laser backwards, it was determined that the asymmetry always remains such that the data are larger than the fit on the high frequency side of the line, where the high frequency side corresponds to a larger Raman shift. For densities above 0.5 amagat and for the pump laser intensities used here, this asymmetry is not consistent with the measured magnitudes of A. C. Stark effects in N_2.[17] At this time we are unable to determine the cause of these asymmetries.

In N_2, both the self-density shifts and the O_2 foreign-gas density shifts were found to lie in the range 50-150 MHz/amagat for the transitions and temperatures discussed above. There was no uniform dependence with either temperature or quantum number J. More importantly, there were inconsistencies observed in both the data acquired during the course of a single day and in the data collected from day-to-day. These inconsistencies have forced us to conclude that the line shift measurements in N_2 are substantially disturbed by the asymmetric lineshapes. The data can, however, be used to establish an upper limit to the magnitude of the line shifts. For all transitions and temperatures indicated for N_2 in Tables I and II, the density lineshifts are less than 150 MHz/amagat. Future elimination of the asymmetry would enable us

to detect lineshifts as small as 10 MHz/amagat with our current experimental apparatus.

The density shifts observed in H_2, unlike those in N_2, were free of the inconsistencies mentioned above. Data for S(1) in H_2 at 295 K are illustrated in Fig. 7, where the density shift is defined as

$$\delta\nu = \nu_R(\rho) - \nu_R(0), \tag{5}$$

where $\nu_R(\rho)$ is the Raman transition frequency at the density ρ. Hence a negative shift results in a smaller Raman frequency. Density shifts were plotted as a function of density difference between the sample and reference cells rather than density because data were collected for reference cell pressures of 50 torr, 100 torr, and 200 torr. The temperature is 295 K for the data of Fig. 7. A summary of our H_2 density shift results is given in Table VI, along with the results from Refs. 16 and 18. The agreement between our results and those of Ref. 18 is consistent with the combined uncertainties for the two experiments.

It should be noted that the density shift for the rotational Raman line in H_2 is substantially different from that observed for the vibrational Raman lines.[14] For example, at 80K, the shift of the Q(1) vibrational transition is 13 times larger than the S(1) rotational Raman line. This difference results from the perturbation of the vibrational frequency of the H_2 molecule during an elastic collision; an effect not present for the rotational transition.

IV. DISCUSSION

A simple qualitative understanding of this temperature dependence for the N_2 rotational Raman broadening data given in Table I can be obtained from a consideration of Anderson's impact theory of the collisional broadening.[19] The linewidth can be expressed as

$$\Delta\nu = n \langle v\sigma(v)\rangle \simeq n \langle v\rangle\langle\sigma(v)\rangle \qquad (6)$$

where n is the molecular number density (cm^{-3}), v is the relative velocity of the collision partners, σ is the collisional broadening cross section, and the brackets denote an average over the velocity distribution of the gas. As can be seen from Eq. 6, the temperature dependence of the density broadening coefficient is implicit in the velocity dependence of the collisional cross section. For example, if we assume a "hard sphere" model for the cross section (velocity independent), the density broadening coefficient ($\Delta\nu/n$) measured in our experiment would be proportional to $T^{0.5}$.

The broadening cross section is composed of contributions from several different type of collisions. Both elastic phase perturbing collisions, and rotationally inelastic collisions contribute to the linewidth. However, there are several cases where the contribution from elastic collisions is small. For example, the linewidths for isotropic vibrational Q branch Raman scattering have no contribution from elastic collisions if collisions perturb the ground and final vibrational level the same amount. This appears to be a good approximation for all cases except hydrogen[14].

Rotational Raman linewidths, on the other hand, have contributions from phase perturbing elastic collisions. This is the primary reason why rotational

Raman transitions usually have larger linewidths than vibrational Raman transitions. However, for the case of N_2, CO, and CO_2, it has been calculated[10] that elastic collisions contribute no more than 15% of the cross section. Therefore, in most cases, the primary problem is to calculate the velocity dependence of the cross section for rotationally inelastic collisions.

The calculation of the collisional cross section has been the subject of considerable research. A good review of the various approaches to this calculation for Raman transitions has been given by Srivastava and Zaidi[20]. One approach to this calculation is to expand the long range part of the intermolecular potential in a multipole expansion[10,19,20], and then calculate the contribution to the cross section of each term in this expansion. Using this approach, Gray and Van Kranendonk[10] have shown that for molecules such as N_2, CO, and CO_2, the most important terms in this expansion for self-broadening are the quadrapole-quadrapole (QQ) potential and the dispersion potential.

It can be shown[19] in general that the velocity dependence of these contributions to the cross section scale as

$$\langle\sigma\rangle \propto \langle v^{-2/(n-1)}\rangle \tag{7}$$

where n is the exponent of the radial dependence of the long range part of the potential in the form $V(r) \sim r^{-n}$. For the QQ potential, n = 5, while for the dispersion potential n = 6. Subsituting Eq. 7 into Eq. 6 and remembering that $v \propto T^{.5}$, we find that the density broadening coefficient should scale with temperature as

$$(\Delta\nu/n) \propto T^{(n-3)/2(n-1)}. \tag{8}$$

From this simple argument, we would expect our density broadening coefficients to scale as $T^{0.25-0.3}$, depending on the relative contribution to the cross section of the QQ and dispersion forces.

To test this simple model of the temperature dependence, we have fit our data in Table I to the equation

$$B = B_o(T/295)^{\gamma} \tag{9}$$

where B_o is the density broadening coefficient at 295 K. The results are given in Table VII as a function of initial rotational state. We find that $0.26 < \gamma < 0.39$, in reasonable agreement with this simple picture. We believe that most of the scatter in γ as a function of J is due to the fact that a much larger temperature range needs to be investigated to accurately determine this small temperature dependence.

However, the scaling given in Eq. 9 may not be valid over a wide temperature range. By theoretically examining temperature dependence of the rotational Raman linewidth over a wide range, Pack[21] proposes a quadratic temperature scaling law for density broadening coefficients that can be written as

$$B = B_o + C_o(T-295) + D_o(T-295)^2 \tag{10}$$

where B_o is the broadening coefficient at 298 K (same as in Eq. 8), and C_o and D_o are fitting coefficients. We have previously used this temperature scaling formula in modeling Raman linewidths in H_2.[14] The data from Table I has been fit to Eq. 10 assuming $D_o = 0$, and the results are also given in Table VII. We find that this expression is just as useful as Eq. 9 in modelling the dependence of the density broadening coefficient over the limited temperature range investigated in our experiment. Both Eqs. 9 and 10 can be used to predict B to better than 3% over the range of 80-300 K. This result emphasizes the need for further measurements at high temperature to accurately determine whether an exponential or quadratic scaling law is appropiate to model the Raman linewidths over a large temperature range.

There are few molecular systems for which the rotational Raman linewidths have been determined as a function of temperature, and no other studies in N_2. However, there have been extensive studies of the temperature dependence of absorption linewidths in CO[22] and CO_2.[23] The absolute magnitude of the linewidths determined from absorption will be different from those determined from Raman scattering. This is due to the fact that different states are involved in the calculation of the collision cross section. However, the temperature dependence will be similar if the same terms in the multipole potential are responsible for the broadening. This is the case[10] for both CO and CO_2 where the most important terms in the potential are the same as for N_2.

Most of the data for linewidths in the literature is given in terms of pressure broadening coefficients. We can compare results by noting that γ in Eq. 9 is related to η by $\gamma = 1 - \eta$, where η is the exponent of the temperature for pressure broadening coefficients. We find that γ for CO and CO_2 absorption linewidths ranges cover a similar range of values as observed for the rotational Raman linewidths for N_2.

The details of the exact theoretical temperature dependence of the rotational Raman linewidths requires an ab initio calculation of the velocity dependence collisional cross section, and is beyond the scope of this study. However, the precision of the data presented here should allow a detailed comparison with linewidths calculated from the various theoretical approaches thus allowing new theoretical advances to be made.

V. CONCLUSIONS

The density self-broadening coefficients have been measured at temperatures of 80 K, 195 K, and 295 K for the even-J rotational Raman transitions in N_2. The temperature dependence of these coefficients was found to fit both linear and T^Y models equally well. The room temperature results of this work are in agreement (less than 5% differences for $J > 2$) with the most recent ab initio calculations. Foreign-gas broadening of these N_2 transitions, due to O_2, was also measured and found to be 10-15% smaller than the self-broadening coefficients. We have also determined that the density self-shifts and O_2 foreign-gas shifts for these same N_2 lines are no larger than 150 MHz/amagat. In a previous letter[2], we have used the above results in the modeling of the temperature dependence of the steady-state Raman gain coefficient in N_2.

The rotational Raman density broadening and shifts in H_2 were measured at 80 K and 295 K. Our results were in general agreement with previous experimental work. This agreement of our H_2 data with other independent measurements provides confidence in the new temperature-dependent N_2 results presented above.

ACKNOWLEDGMENT

This work was supported by the Defense Advanced Research Projects Agency under Contract N00014-8884-C-0256, through the Office of Naval Research.

REFERENCES

1. M. Henesian, C. Swift, and J. R. Murray, "Stimulated Rotational Raman Scattering in Long Air Paths" Opt. Lett. 10, 565 (1985).

2. G. C. Herring, Mark J. Dyer, and William K. Bischel, "Temperature and Wavelength Dependence of the Rotational Raman Gain Coefficient in N_2" (submitted to Opt. Lett.).

3. K. S. Jammu, G. E. St. John, and H. L. Welsh,"Pressure Broadening of the Rotational Raman Lines of Some Simple Gases," Can. J. Phys. 44, 797 (1966).

4. G. V. Milahailov, "The Influence of Temperature and Pressure on the Raman Spectrum of Nitrogen," Soviet Phys. JETP 9, 974 (1959).

5. Yu A. Lazarev, "Line Broadening in Rotational and Rotation-Vibration Raman Spectra of Gases," Opt. Spectry. 13, 373 (1962).

6. F. Pinter, "Dependence of the Width of the Rotational Raman Lines of N_2 and CO_2 on the Quantum Number J," Opt. Spectry. 17, 428 (1964).

7. H. G. M. Edwards, D. A. Long, and S. W. Webb, "Self- and Foreign-Gas Broadening of the Pure Rotational Raman Lines of Oxygen and Nitrogen," Proc. 9th Int. Conf. on Raman Spectrosc. 1984, p. 760.

8. P. Esherick and A. Owyoung, "High-Resolution Stimulated Raman Spectroscopy," in Advances in Infrared and Raman Spectroscopy, Vol. 9, eds., R. J. Clark and R. E. Hester. (Heyden and Sons Ltd., London, 1983).

9. Joseph O. Herschfelder, Charles F. Cartiss, and R. Byron Bird, "Molecular Theory of Gases and Liquids" (John Wiley and Sons, New York, 1954).

10. C. G. Grey and J. Van Kranendonk, "Calculation of the Pressure Broadening of Rotational Raman Lines Due to Multipolar and Dispersion Interaction," Can. J. Phys. 44, 2411 (1966).

11. R. P. Shrivastava and H. R. Zaidi, "Calculation of Self-Broadening Widths of Rotational Raman Lines in H_2 and N_2," Can. J. Phys. 55, 542 (1977).

12. D. Robert and J. Bonamy, "Short Range Effects in Semiclassical Molecular Line Broadening Calculations," J. Phys.(Paris) 40, 923 (1979).

13. R. H. Dicke, "The Effect of Collisions Upon the Doppler Width of Spectral Lines," Phys. Rev. 89 472 (1953).

14. William K. Bischel and Mark J. Dyer, "Temperature Dependence of the Raman Linewidth and Lineshift for the O(1) and O(0) Transition in Normal and para-H_2" (submitted to Phys. Rev. A, 1985).

15. B. K. Gapta and A. D. May, "Dicke Narrowing and Collisional Broadening of the Rayleigh and $S_0(1)$ Raman Line in the Hydrogen Isotopes and H_2-H_e, H_2-N_e Mixtures," Can. J. Phys. 50, 1747 (1972).

16. K. D. Van Den Hout, P. W. Hermans, E. Mazur, and H.F.P. Knapp, "The Broadening and Shift of the Rotational Raman Lines for Hydrogen Isotopes at Low Temperatures," Physica 104A, 509 (1980).

17. R. L. Farrow, and L. A. Rahn, "Optical Stark Splitting of Rotational Raman Transitions," Phys. Rev. Lett. 48, 395 (1982).

18. V. G. Cooper, A. D. May, and B. K. Gupta, "Interferometric Measurements of Line Widths and Frequencies of the $S_0(0)$ and $S_0(1)$ Rotational Lines of H_2," Can. J. Phys. 48, 725 (1970).

19. C. H. Townes and A. L. Schawlow, "Microwave Spectroscopy (Dover, New York, 1975) pg. 368-369.

20. R. P. Srivastava and H. R. Zaidi, "Intermolecular Forces Revealed by Raman Scattering," in Raman Spectroscopy of Gases and Liquids," edited by A. Weber (springer-Verlag, Berlin, 1979) pg. 167-198.

21. Russell T. Pack, "Pressure Broadening of the Dipole and Raman Lines of CO_2 by He and Ar. Temperature Dependence," J. Chem. Phys. 70, 3424 (1979).

22. Jeffrey N-P. Sun and Peter R. Griffiths, "Temperature Dependence of the Self-Broadening Coefficients for the Fundamental Band of Carbon Monoxide," Applied Optics 20, 1691 (1981); Prasad Varanasi and Sunil Sarangi, "Measurement of Intensities and Nitrogen Broadened Linewidths in the CO Fundamental at Low Temperature," J. Quant. Spectrosc. Radiot. Transfer 15, 473 (1975)

23. W. G. Planet and G. L. Tettemer, "Temperature-Dependent Intensities and Widths of N_2 - Broadened CO_2 Lines at 15 μm from Tunable Laser Measurements," J. Quant. Spectrosc. Radiat. Transfer, 22 345 (1979); Lloyd D. Tubbs and Dudley Williams, "Broadening of Infrared Absorption Lines at Reduced Temperatures: Carbon Dioxide," J. Opt. Soc. Am. 62, 284 (1972); R. Ely and T. K. McCubbin, Jr., "The Temperature Dependence of the Self-Broadened Half-Width of the P-20 Line in the 001-100 Band of CO_2," Applied Optics 9, 1230 (1970).

FIGURE CAPTIONS

Figure 1. Schematic of experimental apparatus for quasi-cw stimulated Raman spectroscopy.

Figure 2. Example of S(10) lineshape in N_2 at 195 K for pressures of 10 torr (narrower profile) and 400 torr. Individual dots are data and the solid lines are Voigt fits.

Figure 3. S(10) linewidths in N_2 at temperatures of 80 K (□),195 K(○), and 295 K (Δ). Solid lines are linear least square fits to the data.

Figure 4. J dependence of the N_2 rotational Raman broadening coefficients for 80 K (□), 195 K (○), and 295 K(Δ).

Figure 5. Comparison of theoretical calculations with experimental data for collisional broadening of the rotational Raman lines in N_2 at room temperature. The calculations are from Ref. 10 (long dash), Ref. 11 (short dash), and Ref. 12 (solid line). The experimental data are from Ref. 3 (□) and this work (Δ).

Figure 6. Lorentzian (□) and Gaussian (Δ) components from Voigt fits to data as a function of density for S(1) in H_2. Solid line is a linear one parameter fit to Eq. 1.

Figure 7. Example of data for lineshift determination for S(1) in H_2 at 295 K. The solid line is the least squares fit.

TABLE I. Temperature dependence of the self-broadening coefficients for the rotational Raman lines of N_2.

	B (MHz/amagat)		
S(J)	295 K	195 K	80 K
0	-	4730 ± 700	3140 ± 470
2	4160 ± 400	3560 ± 350	2700 ± 270
4	3580 ± 60	3230 ± 320	2490 ± 250
6	3560 ± 30	3070 ± 30	2520 ± 40
8	3270 ± 60	2860 ± 30	2120 ± 60
10	3060 ± 60	2660 ± 30	1940 ± 40
12	2870 ± 50	2340 ± 260	1690 ± 100
14	2660 ± 270	2150 ± 215	-
16	-	1840 ± 185	-

TABLE II. Temperature dependence of the foreign-gas (O_2) broadening coefficients of N_2 rotational Raman lines.

	B(MHz/amagat)	
S(J)	295 K	195 K
6	2970 ± 130	2690 ± 120
8	2770 ± 80	2600 ± 100
10	2750 ± 50	2410 ± 100
12	2450 ± 70	1980 ± 100

TABLE III. Comparison of different measurements of the room temperature self-broadening in N_2.

S(J)	B (MHz/amagat)			
	Present Work	Ref. 3	Ref. 6	Ref. 7
2	4160 ± 400	3370		
4	3580 ± 60	3050	2590	3280 ± 300
6	3570 ± 30	3050		
8	3270 ± 60	2660	2300	3150 ± 300
10	3070 ± 60	2590		
12	2870 ± 50	2400	1980	2820 ± 300
14	2660 ± 270	2205		
16		2080		

TABLE IV. H_2 rotational Raman parameters for an ortho:para ratio of 3:1.

T (K)	S(J)	ν_R (cm^{-1})	$\Delta\nu_D$ (MHz)	D_o[a] (cm^2 amagat sec^{-1})	A (MHz amagat)	ρ_c (amagat)
80	0	354	48	.871	1.37	0.095
	1	587	80	.493	2.10	0.088
295	0	354	92	1.19	1.87	0.068
	1	587	153	1.42	6.15	0.134

[a]Reference 14

TABLE V. Self-broadening coefficients for the rotational Raman lines of H_2.

	B (MHz/amagat)				
	295 K			80 K	
S(J)	This Work	Ref. 16	Ref. 18	This Work	Ref. 16
0	77 ± 2	84 ± 2	84 ± 2	67 ± 2	63 ± 1
1	114 ± 5	104 ± 2	105 ± 4	110 ± 3	99 ± 1

TABLE VI. Temperature dependence of the density lineshifts for H_2 rotational Raman lines.

	$\delta\nu = \nu_R(\rho) - \nu_R(0)$ (MHz/amagat)			
	295 K		80 K	
S(J)	This Work	Ref. 18	This Work	Ref. 16
0	6.5 ± 3	3.1 ± 1.5	- 22.3 ± 0.6	- 22.3
1	5.9 ± 1	4.0 ± 1.5	- 23.0 ± 0.6	- 17.8

TABLE VII. Fit parameters for temperature dependence of density self-broadening coefficients in N_2.

S(J)	B_o (MHz amagat^{-1})	γ	C_o (MHz amagat^{-1}K^{-1})
2	4160	0.33 ± 0.02	6.8 ± .4
4	3580	0.28 ± 0.01	5.1 ± .7
6	3560	0.26 ± 0.04	4.8 ± .1
8	3270	0.33 ± 0.004	5.4 ± .7
10	3060	0.35 ± 0.002	5.2 ± .6
12	2870	0.39 ± 0.03	5.4 ± .1

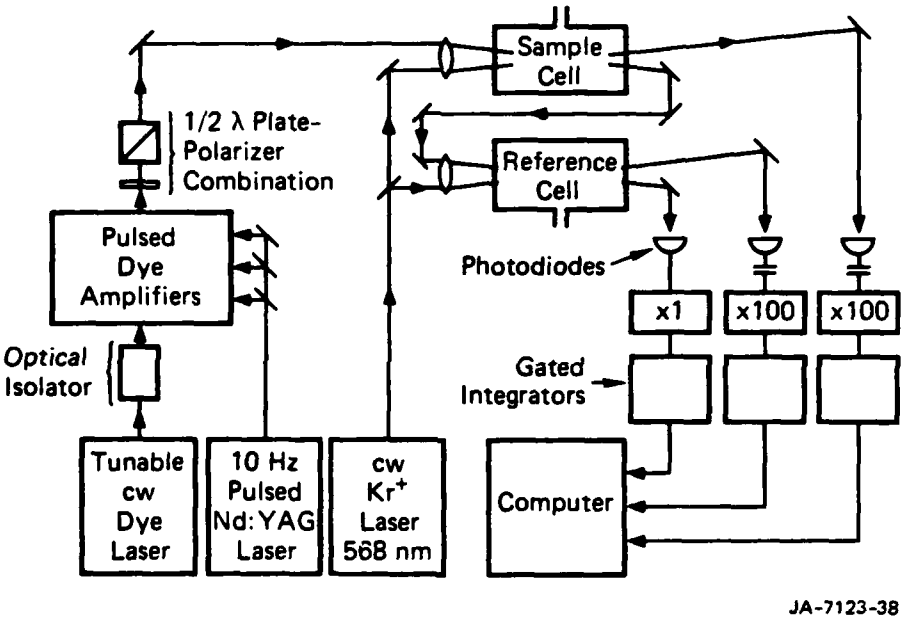
Sample Cell
1/2 λ Plate-Polarizer Combination
Reference Cell
Pulsed Dye Amplifiers
Photodiodes
x1
x100
x100
Optical Isolator
Gated Integrators
Tunable cw Dye Laser
10 Hz Pulsed Nd:YAG Laser
cw Kr+ Laser 568 nm
Computer
JA-7123-38

Figure 1

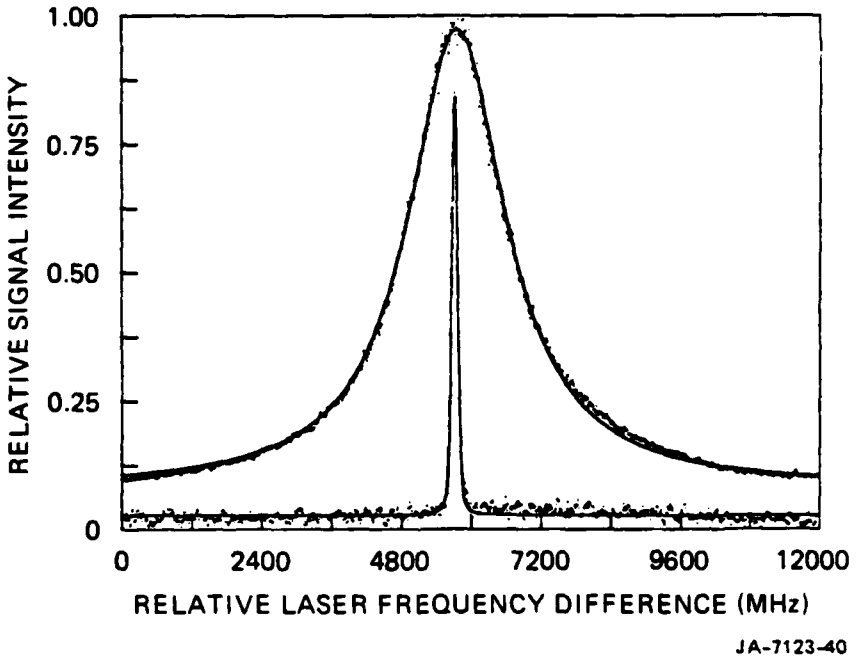
1.00
0.75
0.50
0.25
0
RELATIVE SIGNAL INTENSITY
0
2400
4800
7200
9600
12000
RELATIVE LASER FREQUENCY DIFFERENCE (MHz)
JA-7123-40

Figure 2

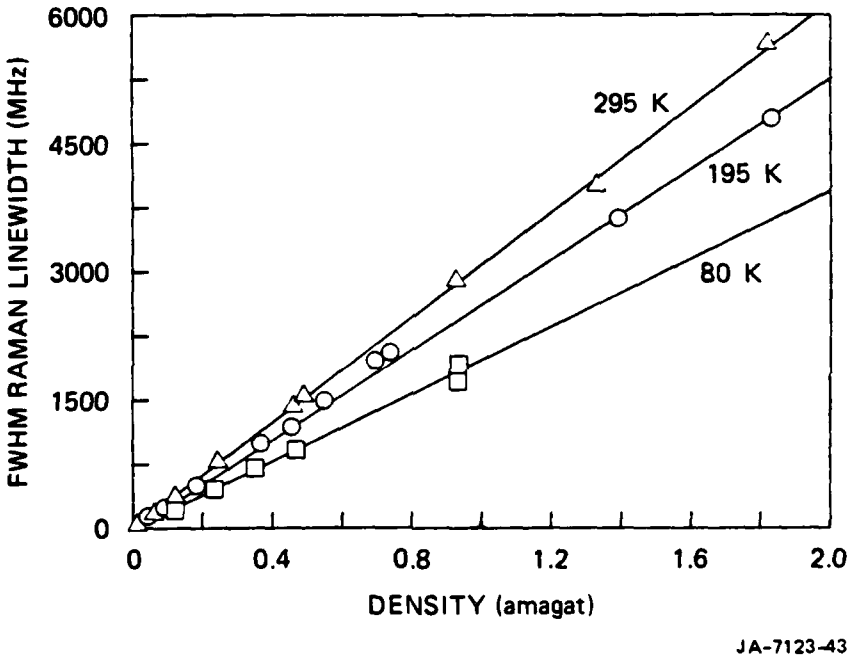
6000
4500
3000
1500
0
FWHM RAMAN LINEWIDTH (MHz)
295 K
195 K
80 K
0
0.4
0.8
1.2
1.6
2.0
DENSITY (amagat)
JA-7123-43

Figure 3

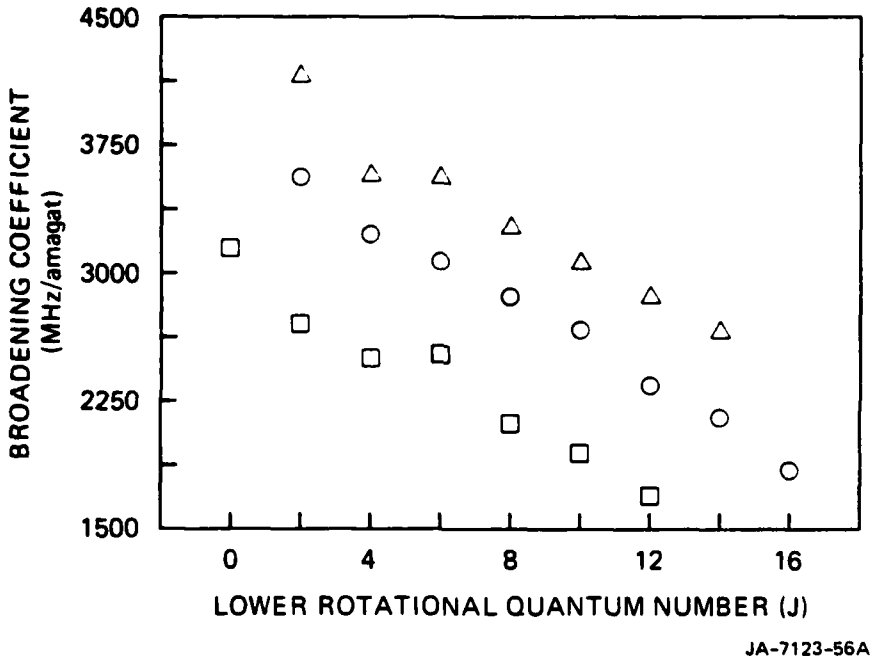
4500
3750
3000
2250
1500
BROADENING COEFFICIENT
(MHz/amagat)
0
4
8
12
16
LOWER ROTATIONAL QUANTUM NUMBER (J)
JA-7123-56A

Figure 4

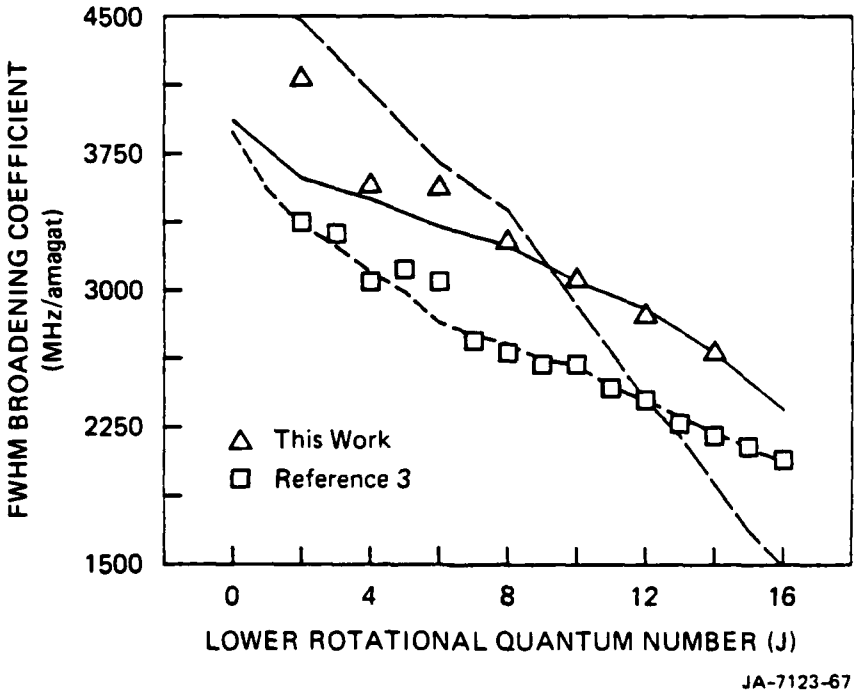
4500
3750
3000
2250
1500
FWHM BROADENING COEFFICIENT
(MHz/amagat)
This Work
Reference 3
0
4
8
12
16
LOWER ROTATIONAL QUANTUM NUMBER (J)
JA-7123-67

Figure 5

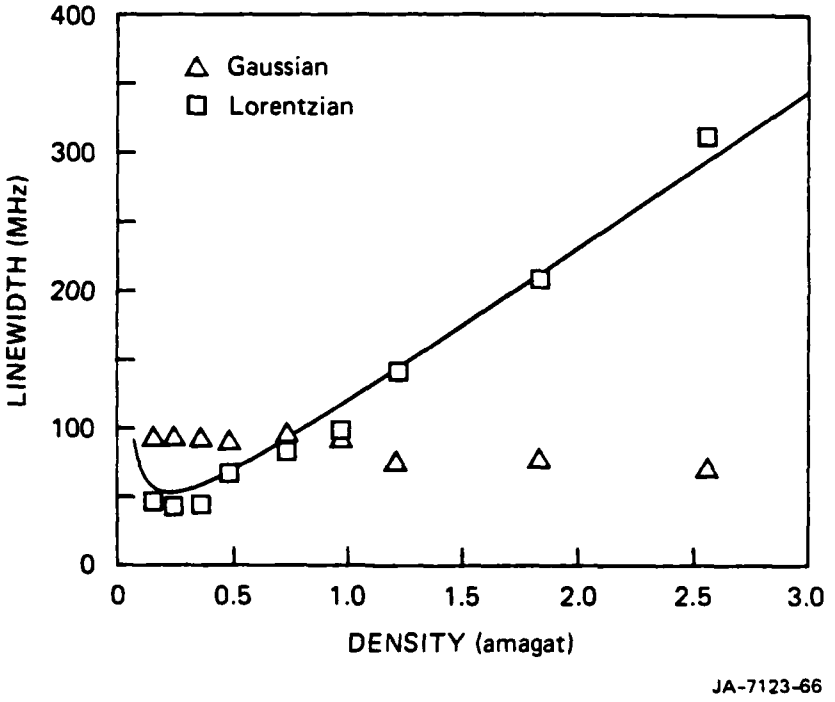
400
300
200
100
0
LINEWIDTH (MHz)
Gaussian
Lorentzian
0
0.5
1.0
1.5
2.0
2.5
3.0
DENSITY (amagat)
JA-7123-66

Figure 6

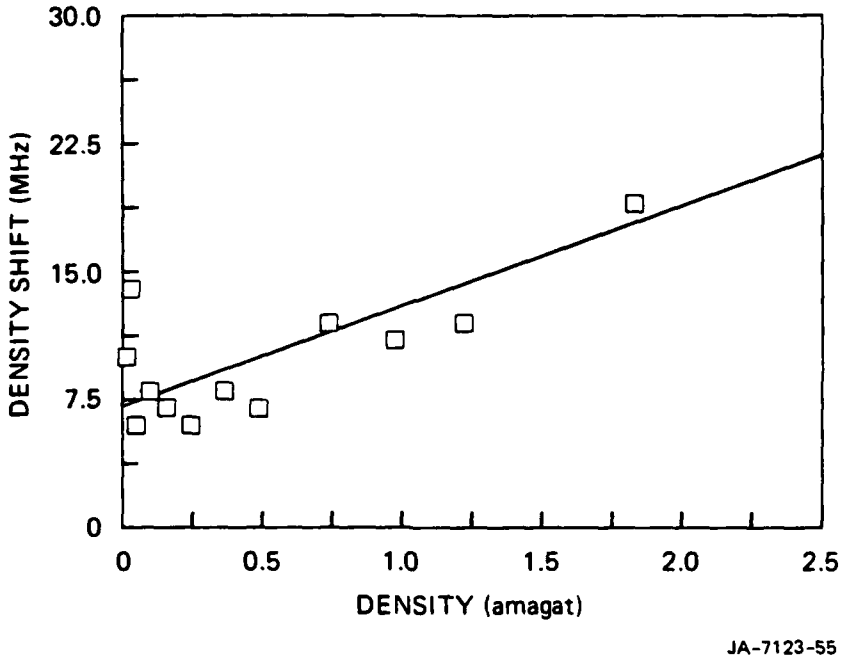
30.0
22.5
15.0
7.5
0
DENSITY SHIFT (MHz)
0
0.5
1.0
1.5
2.0
2.5
DENSITY (amagat)
JA-7123-55

Figure 7